Energy Systems
https://doi.org/10.1007/s12667-024-00672-w

ORIGINAL PAPER

Reliability-based sizing of islanded multi-energy microgrid: a conic chance-constrained optimization approach

Juan Camilo Camargo-Berrueco[1] · **Diego Adolfo Mejía-Giraldo**[1] · **Santiago Lemos-Cano**[2]

Received: 5 August 2022 / Accepted: 13 March 2024

Abstract

This paper presents a methodology to optimally design a multi-energy microgrid with thermal and electric loads considering $N-1$ and probabilistic regulation reserves. This methodology consists of a chance-constrained optimization that determines the optimal sizing of the microgrid. Microgrid operations are rigorously considered by modelling hourly thermal and electric demand patterns as well as technology production schedules over a year. Such schedules include both electric and thermal power balances, ramp constraints, $N-1$ and regulation reserves, among others. To ensure a reliable microgrid design and operation, reserve constraints have been proposed to deal with both $N-1$ generation contingencies, and forecast errors. $N-1$ reserves guarantee that a sudden outage of any of the electric generators is strategically covered by the remaining generators in order to avoid load shedding. Additionally, nonzero-mean random forecast errors of electric load and solar production are addressed by a set of chance constraints able to schedule asymmetric up and down regulation reserves. Their levels are high enough to cover hourly random forecast errors (or intermittencies) with a high threshold probability. The proposed methodology results in a mixed integer second-order cone program. Results of microgrid designs with and without reliability reserves are carefully analysed and compared. Neglecting reliability constraints leads to a lower-cost design at the expense of exposing the microgrid to unsafe operation. Finally, sensitivity analysis to study the optimal portfolio sizing with respect to electric BESS investment cost, solar production forecast mean error, and random intermittency threshold probability are performed.

Keywords Multi-energy microgrid sizing · MISOCP · $N-1$ security criterion · Regulation reserves · Chance-constraint · Reliability constraints

Extended author information available on the last page of the article

Published online: 14 April 2024

List of symbols

Sets and indexes

$\mathcal{G}$	Fuel-fired conventional generator: ICE, MT and DSL. Subscript g.
$\mathcal{J}$	Generation technologies: Solar (PV), Internal-Combustion Engine (ICE), Diesel (DSL), micro turbine (MT). Subscript j
$\mathcal{K}$	All the available technologies in the MG ($\mathcal{J} \cup \mathcal{S} \cup N$): PV, ICE, DSL, MT, EC, AC, TESS and BESS. Subscript k
$\mathcal{N}$	Thermal energy technologies: Electric Chiller (EC), Absorption Chiller (AC). Subscript n
$\mathcal{S}$	Energy Storage Systems: Battery (BESS), Thermal Storage (TESS). Subscript s
$\mathcal{T}$	Time-step Set. Subscript t
Y	Lifespan for microgrid. Subscript y

Parameters

β^R	Reserve cost for $N-1$ and regulation reserves $\left[\frac{\$}{\text{kW}}\right]$
Δt	Steplength for each considered timestep $[h]$
δ_s^{sd}	Hourly self-discharge factor for storage s [%]
η_s^{rt}	Round-trip efficiency for storage s [N.A.]
η_{pv}	Derating factor (Efficiency) of the PV system [N.A.]
$\eta_t^{+(-)}$	Violation probability to regulation reserve requirement during the time t
γ	Yearly OPEX scale factor [N.A.]
ω_k	CO_2 emissions tax for technology $k \left[\frac{\$}{kg}\right]$
ϕ_j	Heat recovery factor per kW to generator $j \left[\frac{kW}{kW}\right]$
π_g	Fuel price to operation of generator $g \left[\frac{\$}{MBTU}\right]$
ρ_n	Coefficient of performance of chiller n [N.A.]
$\underline{\mu}_s^{\text{SOC}}, \overline{\mu}_s^{\text{SOC}}$	Min and Max operational limit for state-of-charge to storage s [p.u.]
$\underline{\mu}_j$	Minimal operational limit for generator j [p.u.]
$\underline{\mu}_n$	Minimal operational limit for chiller n [p.u.]
$\varepsilon_{D,t}$	Forecasting error for demand in the time t
$\varepsilon_{pv,t}$	Forecasting error for pv production in the time t
ε_t	Net Forecasting error in the time t
a_g	Slope for the fuel rate curve for fuel-fired generator g $\frac{\text{MBTU}}{kWh}$
b_g	Y-intercept for the fuel rate curve for fuel-fired generator g $\frac{\text{MBTU}}{h}$
C_T	Temperature coefficient for PV-system $\left[\frac{\%}{^\circ C}\right]$
D_t^{el}	Electric load demand to microgrid in time t [kW]
$E_{\text{BESS}}^{\text{lt}}$	Energy throughput for the BESS technology [kWh]
$ER_k^{CO_2}$	CO_2 emissions rate for technology $k \left[\frac{\text{kg}}{\text{kWh}}\right]$

G_{stc}	Standard condition solar radiation $\left[\frac{kW}{m^2}\right]$
G_t	Solar radiation in time $t\left[\frac{kW}{m^2}\right]$
I_n^{chi}	Investment cost to chiller $n\left[\frac{\$}{kW}\right]$
I_j^{gen}	Investment cost to generator $j\left[\frac{\$}{kW}\right]$
$I^{\text{sto,E}}$	Investment cost per kWh for storage $s\left[\frac{\$}{kWh}\right]$
$I_s^{\text{sto,p}}$	Investment cost per kW to storage $s\left[\frac{\$}{kW}\right]$
M	Large value [N.A.]
$N_{\text{BESS}}^{\text{lt}}$	Average cycles to failure [N.A.]
$OM_k^{\text{var(fix)}}$	Variable (fixed) OM cost for technology $k\left[\frac{\$}{kW}\right]$
Q_t^{load}	Cooling load demand to microgrid in time t [kW]
Q_t^H	Heat load demand at time $t\,[kW-]$
$q_{t,1-\eta^{+(-)}}^{+(-)}$	$1-\eta$ quantile for the positive(negative) forecasting error distribution
r	The discount rate used to compute Net Present Value
$r_j^{\text{up}}, r_j^{\text{down}}$	Maximum ramp up and down for power output change in generator j
T_t^{amb}	Ambient temperature in time $t\,[^\circ C]$
T_t^{mod}	Actual PV system cells temperature $[^\circ C]$
T^{OpNom}	Nameplate operational temperature for PV system cells $[^\circ C]$

Variables

$\Delta p_{\text{BESS},t}^{\text{SR}+(-)}$	Up(Down) Regulation reserve for BESS at time t [kW]
$\Delta p_{j,t}^{\text{SR}+}$	Up/Down regulation reserve for generator j at time t [kW]
$\Delta p_{\text{BESS},t}^{S}$	$N-1$ security reserve for BESS against contingency in time t [kW]
$\Delta p_{j,t}^{S}$	$N-1$ security reserve for generator j against contingency in time t [kW]
$\omega_{\text{BESS},t}$	Wear cost for BESS technology during time-step t
$\text{CO}_{k,t}$	Carbon emission tax for technology k during time-step t
$\text{OM}_{k,t}$	Operation and maintenance cost for the technology k during time-step t
$\text{SR}_t^{+(-)}$	Positive (negative) estimated regulation reserve requirements during time t
e_s^{nom}	Nominal energy capacity to storage s [kWh]
$e_{s,t}^{\text{SOC}}$	State-of-charge of storage system s in time t [kWh]
$F_{g,t}$	Fuel cost for the fuel-fired generation g during time t
$p_{s,t}^{\text{ch(dis)}}$	Power charged(discharged) to storage s in time t [kW]
p_j^{nom}	Nominal power output for generator j [kW]
p_s^{nom}	Nominal charge/discharge power input/output to storage s [kW]
$p_{j,t}$	Power output from generator j in time t [kW]
q_n^{nom}	Nominal power output for chiller n [kW]

$q_{n,t}$	Cooling power from cooling technology n in time t [kWh]
$z_{s,t}^{\text{ch(dis)}}$	Binary charge (discharge) power input for storage s in time t
$z_{j,t}$	Binary power output decision for technology j in time t
$z_{n,t}$	Binary power output decision for chiller n in time t

Abbreviations

AC	Absorption chiller
BESS	Battery energy storage systems
CAPEX	Capital expenditures
CO_2	Carbon dioxide
EC	Electric chiller
IDEAM	Instituto de Hidrología, Meteorología y Estudios Ambientales
MISOCP	Mixed integer second-order cone programming
MILP	Mixed-integer linear programming
MT	Microturbine
O[MYAMP	M] Operation and maintenance
OPEX	Operational expenditures
PV	Photovoltaic system
SOC	State-of-charge
RMG	Reconfigurable microgrid
TESS	Thermal energy storage systems
WT	Wind turbines

1 Introduction

Renewable energies have become essential sources of electricity when it comes to the construction of microgrids around the world [1]. Several factors like increasing fuel prices of conventional generation, decreasing installation costs of renewable energy [2], and environmental concerns have promoted their use. Even with such drivers, in order to support microgrid deployment, several challenges such as optimal sizing and operation, optimal control strategies, and reliability supply, need to be addressed [3].

1.1 Motivation

Although the microgrid planning should consider estimates of both energy resources availability and demand, it is determined by the size of its elements (generators and storage systems). The sizing process, in turn, relies on the adopted operational strategy of the microgrid and data assumptions. Operational aspects are considered during the microgrid sizing phase to account for the operational conditions that will be employed during operation. Although the exact operational condition is not perfectly known during the sizing phase, considering operational constraints ensures that the microgrid is properly sized and thus the operational strategies can be feasible. In general, determining the "appropriate" size of components for a given set

of electrical and/or thermal load profiles, remains a challenge. If components are oversized, the system capital cost and energy curtailment will be unnecessarily high. Also, generator may reach lower efficiency and higher maintenance costs which may lead to low generator reliability as fuel-fired diesel generators can develop "wet-stacking" at low power output w.r.t to rated capacity [4, 5]. If components are undersized continuous load shedding, unsatisfied demand and high non-renewable energy generation may occur leading to unsuccessful operation [6]. Thus, in order to guarantee a continuous and reliable energy supply to the users, an optimal sizing methodology requires a rigorous modeling of operational aspects in short time frames. Sudden outages of technologies supplying energy to the microgrid as well as intermittence and uncertainties in both solar photovoltaic energy production and demands are essential elements to consider to guarantee a reliable and economic microgrid performance.

In this paper, a Mixed Integer Second-Order Cone Programming (MISOCP) model for jointly optimizing the sizing and operation of an islanded multi-energy microgrid is presented. The type of microgrids subject to study in this work is one that is not connected to the power grid and considers both thermal and electric loads on an hourly basis. The microgrid is designed considering a portfolio of distributed energy resources to deliver thermal energy and electricity to a set of thermal and electric loads commonly observed in hotel facilities. This portfolio includes conventional generation resources as internal combustion engines, microturbines and diesel-fueled generator, renewable generation resources as solar PV modules, energy storage systems such as batteries and thermal storage, and cooling supplying technologies such as both absorption and electric chillers. Additionally, in order to ensure a reliability-based microgrid design, the $N-1$ security criterion has also been included in the proposed optimization model. Finally, with the aim of guaranteeing continuous supply–demand balance, even during random fluctuations of demand and/or intermittent generation, a set of probabilistic chance constraints are imposed to schedule an appropriate level of hourly regulation reserves.

1.2 Literature review

The reliability-based optimal sizing of multi-energy microgrids is investigated in this paper. Although scientific literature related to microgrid planning has traditionally focused on its operation and sizing, reliability criteria are not usually contemplated. In [7] authors present an optimal islanded microgrid planning with BESS. The BESS is scheduled as reserve provider. The BESS, defined by both, energy capacity and rated power, is defined as the maximum difference between pre-defined regulation reserves and power margin of committed units. Notwithstanding, reserve requirements are not estimated as a function of microgrid size, but they are considered as an input model parameter. In [8], authors present a computational framework to evaluate both economic and resilience in microgrid planning without considering reserve estimation. This work is extended in [9] to evaluate cooling and heating load, along with CHP systems, notwithstanding, reserves are not scheduled. Authors in [10] present a model to optimally size an electric microgrid using a multiyear

approach. The BESS degradation is considered as a function of the hourly power-to-energy ratio. Detailed multi-year simulations spanning the entire lifetime of the project at an hourly basis are considered and the model is solved using an iterative MILP-solving strategy. Regulation reserves are computed as a portion of the load and expected renewable production to account for the uncertainties. However, neither cooling loads nor $N-1$ reserves are modeled. In [11] a stochastic optimisation model for isolated multi-energy systems sizing is presented. Hydrogen and heat loads are considered. A tractable representation of a fully linear AC power flow equations were presented in the planning model. Authors do not model $N-1$ and regulation reserves requirements. Authors of [12] presented a two-step Mixed-Integer Linear Programming (MILP) approach to determine the optimal sizing of a rural islanded microgrid in which four representative weeks are employed to describe one operating year; neither thermal demand nor reliability constraints were considered. In the work [13], a hybrid genetic algorithm-MILP approach is employed to find the optimal sizing of components of an islanded microgrid that delivers power to a hotel. The microgrid sizing is determined by the genetic algorithm; whereas the operational problem, that schedules technology production, is handled by a MILP model. The work [14] considers thermal and hydrogen loads. In order to reduce computational burden, twelve representative days (out of 365 days per year) are considered; $N-1$ reserves are out of the scope of this work. In [15, 16] and [17] authors aim to find the optimal size of an islanded microgrid operating. Uncertainties in electric and thermal demand are neglected. The sizing problem is tackled by a grid-search heuristic algorithm; and the operational problem is solved employing a MILP model over a 12-hour control horizon. These two problems are solved independently, i.e., there is no joint optimization between the sizing and operation problems, and operational reliability aspects are not addressed. In [18] a MILP model is presented to design either grid-tied or islanded microgrids. Thermal and electrical loads are assumed as known. The sizing and operating strategies are based on minimization of capital, operation, and maintenance costs of the selected technologies. This work has considered the existence of a thermal and an electric network; nevertheless, power reserves to cover component outages have not been considered. Reference [19] presents a MILP model to jointly optimize sizing and operation of an islanded electric microgrid via minimization of net present cost; Operational reliability aspects have not studied.

In terms of microgrid operations, several investigations have employed chance-constraints to define optimal regulation reserve levels. These reserves allow the microgrid to have enough available energy to deal with random generation-demand balance fluctuations due to forecast errors or intermittency in renewable generation. For instance, the authors of [20] present a probabilistic approach to estimate regulation reserves based on the forecast error distribution of the PV and WT system outputs and demand. Reserves are estimated to deal with random events as generation intermittency, forecasting errors, and generation outages, while minimizing the expected energy not supplied of the microgrid. This study assumes the microgrid is already designed. In [21] authors present the concept of probability of successful

islanding as the probability to cover a sudden islanding with microgrid scheduled reserves. Chance constraints based on the three-sigma rule impose conditions to estimate an amount of reserves that cover at least 99% of possible forecast deviations. A normal probability distribution of forecast errors of wind, PV and load is modeled; however, the optimization model does not find optimal microgrid sizing, but it does optimize the operation without considering the $N-1$ security criterion. In [22], an operational scheduling model using probabilistic chance constraints is proposed to cover the uncertainty of demand and renewable resources. A method for allocating reserves to a microgrid is presented in order to deal with prediction errors and potential failures in both distributed generation and battery systems, maintaining power balance with a high probability depending on the parameter L^{req}. Estimated reserves are allocated to avoid load shedding when events such as materialization of forecast errors, BESS outages or unexpected islanding occur. Given that microgrid sizing is not considered, the availability of reserves is fixed. This in turn makes difficult to maintain power balance with high probabilities. In contrast, our work focuses on properly sizing the microgrid as a function of the probability of maintaining power balance.

The work presented in [23] is similar to the work [22] in the sense that it assumes that the microgrid has already been sized. This constitutes the first key difference w.r.t our work. Second, the work [23] does not allocate reserves to deal with potential generator or storage system outages. And third, authors [23] did not take into account the amount of energy available in the storage system when defining reserves. This could lead the storage system being allocated with upward (downward) reserves that could not be implemented if its current state of charge is low (high).

A variety of investigations on microgrid sizing guaranteeing $N-1$ security criteria have also been reported. Generator outages are modeled to avoid power not served during post-contingency states. Remaining online generators are forced to adjust their output to support the power of the faulted generator. This can be done only if reserves have been properly scheduled. Authors in [24] developed a mixed-integer quadratically constrained quadratic programming to jointly optimize sizing and operation of an isolated microgrid introducing $N-1$ security constraints; however, they do not schedule regulation reserves to handle renewable intermittencies and demand uncertainties. The work [25] is an extension of the work from [18] and their results ensure a secure optimal microgrid design. The generator contingencies modeled in [24] and [25] consider the loss of a single generating unit within a power plant. But, in order to consider a more extreme situation and thus achieve a robust operation, this work has modeled the outage of the entire generation plant. Also, none of these investigations have addressed the challenge of random fluctuations in demand and renewable generation in short time frame during microgrid operations.

Table 1 Summary of the most relevant formulation in the literature

Ref	Oper. strategy	Solution method	Design approach		Energy			Reserves constraints	
			Sizing	Operation	Electric	Cooling	Heating	$N-1$	Regulation
[9]	Opt-based	Optimal	✓	✓	✓	✓	✓		
[10]	Opt-based	Iterative	✓	✓	✓				✓
[11]	Opt-based	Optimal	✓	✓	✓		✓		
[12]	Both	Both	✓	✓	✓				
[14]	Opt-based	L & F*	✓	✓	✓	✓	✓		
[15–17]	Both	Heuristic	✓	✓	✓	✓			
[18]	Opt-based	Optimal	✓	✓	✓	✓	✓		
[19]	Rule-based	Heuristic	✓	✓	✓				
[20]	Opt-based	Optimal		✓	✓			✓	✓
[21]	Opt-based	Optimal		✓	✓				✓
[22]	Opt-based	Optimal		✓	✓			✓	✓
[23]	Opt-based	Optimal		✓	✓				✓
[24]	Opt-based	Optimal	✓	✓	✓	✓	✓	✓	
[25]	Opt-based	Optimal	✓	✓	✓	✓	✓	✓	
This Work	Opt-based	Optimal	✓	✓	✓	✓	✓	✓	✓

*Leader and Follower Method

Table 1 shows a summary of the discussed approaches in the scientific literature in the microgrids field. The table focuses on highlighting the key differences among them and displays the research gaps addressed in this manuscript.

1.3 Contribution

To the best of our understanding, the existing literature does not provide a comprehensive optimization model for both sizing and operating a multi-energy microgrid that, at the same time, addresses the reserves provisions against both (demand and solar PV) forecast deviations and sudden outage of any generation resource in isolated microgrids. To fill these research gaps, this paper presents a methodology to optimally design a hybrid multi-energy microgrid (with thermal and electric loads) that considers both $N-1$ and regulation reserves and minimizes the net present CAPEX and OPEX. The $N-1$ criterion, traditionally employed to guarantee that demand is always met, even under the outage of any generation resource, is modeled to determine enough reserves to avoid load shedding under sudden generator outages. Up and down regulation reserves are estimated using chance constraints to cover joint random fluctuations of demand and solar PV with respect to their forecasted values.

The main contributions from this work are as follows:

- The proposal of a MISOCP model to jointly optimize reliability-based design, sizing and operation of an islanded multi-energy microgrid with both thermal and electric load.
- The design and inclusion of a set of constraints to ensure a reliable thermal-electric microgrid operation by optimally combining two types of reserves. One type of reserves is in charge of maintaining continuous enough energy supply against $N-1$ electric generator contingencies. And the regulation reserves are computed by employing a set of hourly probabilistic chance constraints to guarantee enough asymmetric power and energy reserves to deal with nonzero-mean random forecast errors of both demand and solar PV generation. Positive and negative errors are rigorously differentiated to schedule asymmetric up and down regulation reserves respectively.

The remainder of this work is organized as follows: Sect. 2 presents the mathematical proposed model for reliability-constrained design and operation of microgrid. Section 3 presents the case study and its results are discussed in Sect. 4. Finally, Sect. 5 presents conclusions for this paper.

2 Proposed model

In this section we introduce the proposed mathematical model for selecting, sizing and operating the microgrid architecture displayed in Fig. 1, which is supposed to satisfy both electricity and thermal demands. To achieve this, we have considered a generic architecture in which relations between thermal and electrical systems is also modeled. The proposed sizing model is in charge of determining the required components and its size that guarantee demands satisfaction in a secure manner at minimum cost. Additionally, a set of reserve requirements is considered. The resulting problem is a MISOCP.

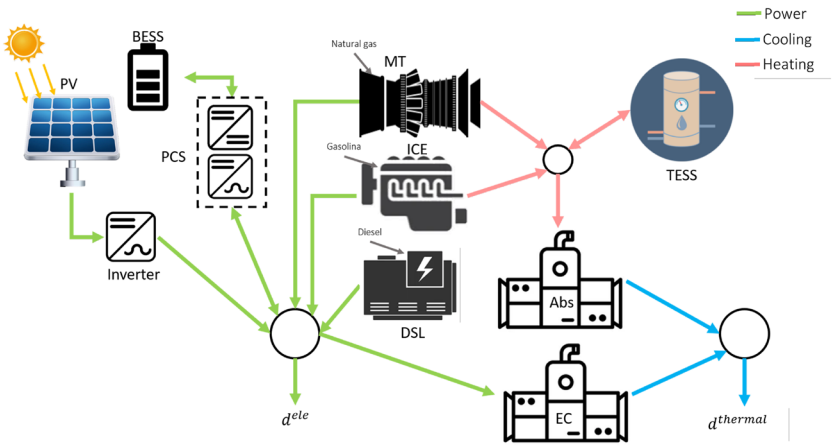

Fig. 1 Base microgrid architecture

2.1 Objective function

The proposed microgrid sizing model is aimed to minimize the total investment cost (CAPEX) of components and discounted operational cost (OPEX) as represented in Eq. (1).

$$\text{minimize} \quad \left(\text{CAPEX} + \sum_{y \in Y} \frac{\gamma \, \text{OPEX}}{(1+r)^y} \right) \tag{1}$$

where factor γ is the ratio of the number of hours per year (8760) to the number of hours employed to represent the operations of the microgrid $|\mathcal{T}|$, i.e., $\gamma = \frac{8760}{|\mathcal{T}|}$.

2.1.1 Capital expenditures

Capital costs are considered at year zero. The capital cost of generation technologies is computed as the product of generator size p_j^{nom} (in kW) and the corresponding unit investment I_j^{gen} (in \$/kW). Likewise, investment cost of chillers is determined as the product between nominal capacity q_n^{nom} (in kW) and unit cost I_n^{chi} in (\$/kW). Investment cost of energy storage systems depends on both rated power output p_s^{nom} (in kW) and nominal storage capacity e_s^{nom} (in kWh). Total CAPEX is presented in Eq. (2):

$$\begin{aligned} \text{CAPEX} = & \sum_{j \in \mathcal{J}} I_j^{\text{gen}} p_j^{\text{nom}} + \sum_{n \in N} I_n^{\text{chi}} q_n^{\text{nom}} \\ & + \sum_{s \in \mathcal{S}} \left(I_s^{\text{sto,P}} p_s^{\text{nom}} + I_s^{\text{sto,E}} e_s^{\text{nom}} \right) \end{aligned} \tag{2}$$

2.1.2 Operating expenditures

Total operational microgrid expenditures are presented in Eq. (3):

$$\text{OPEX} = \sum_{t \in T, g \in \mathcal{G}} F_{g,t} + \sum_{t \in T, k \in \mathcal{K}} \left[\text{OM}_{k,t} + \text{CO}_{k,t} \right] + \sum_{t \in T} \left[w_{\text{BESS},t} + \text{RC}_t \right] \tag{3}$$

where $F_{g,t}$ represents fuel cost (Eq. (4)). Fuel price π_g of fuel-fired technology g is given in $\left[\frac{\$}{\text{MBTU}} \right]$. Thus, the affine function $a_g p_{g,t} + b_g z_{g,t}$ denotes fuel consumption. Parameters a_g and b_g in $\left[\frac{\text{MBTU}}{\text{kWh}} \right]$ and $\left[\frac{\text{MBTU}}{\text{h}} \right]$, respectively are employed to estimate fuel consumption from the fuel rate curve for fuel-fired power plants with power output $p_{g,t}$ and scheduled operation defined by variable $z_{g,t}$. Operation and maintenance cost $\text{OM}_{k,t}$ is shown in Eq. (5). OM_k^{var} and OM_k^{fix} are the variable and fixed operational cost rates, respectively, scaled by power output ($p_{j,t}$ or $p_{s,t}^{\text{dis}}$).

Carbon emissions tax $\mathrm{CO}_{g,t}$, displayed in Eq. (6), require emissions tax rate ω_g imposed by the market. Parameter $\mathrm{ER}_g^{CO_2}$ in $\left[\frac{kg}{\mathrm{kWh}}\right]$ represents the emissions factor for each technology [18, 26, 27]. Electric battery degradation cost, denoted by $w_{\mathrm{BESS},t}$, is computed according to Eq. (7). The operational cost is considered to account for its degradation in storage capacity. It is assumed that the BESS will be replaced once its overall energy throughput E_{BESS}^{lt} is reached [28, 29]. Energy throughput can be parameterized as a number of average"effective" cycles to failure, i.e., $E_{\mathrm{BESS}}^{\mathrm{lt}} = N_{\mathrm{BESS}}^{\mathrm{lt}} e_s^{\mathrm{nom}}$. Reference [29] shows that $N_{\mathrm{BESS}}^{\mathrm{lt}}$ depends on the average product between depth of discharge and cycles to failure. Then, degradation cost per unit of cycled energy, computed as $I^{\mathrm{sto,E}} e_s^{\mathrm{nom}} / E_{\mathrm{BESS}}^{lt}$ needs to be multiplied by BESS discharge power $p_{\mathrm{BESS},t}^{\mathrm{dis}}$ (affected by efficiency) to obtain the dollar amount of total degradation cost $w_{\mathrm{BESS},t}$ as in Eq. (7). Reserve cost RC_t is computed as the product of the sum of all reserves each time-step —down regulation reserves, up regulation reserves and $N-1$ reserves— by the reserve price β^R as shown in (8).

$$F_{g,t} = \pi_g \left(a_g p_{g,t} + b_g z_{g,t} \right) \Delta t, \quad \forall g \in \mathcal{G} : \mathcal{G} \subseteq \mathcal{J}, t \in T \tag{4}$$

$$\mathrm{OM}_{k,t} = \mathrm{OM}_k^{\mathrm{var}} p_{k,t} + \mathrm{OM}_k^{\mathrm{fix}} p_k^{\mathrm{nom}}, \quad \forall k \in \mathcal{K}, t \in T \tag{5}$$

$$\mathrm{CO}_{g,t} = \omega_k \, \mathrm{ER}_g^{\mathrm{CO}_2} \, p_{g,t} \, \Delta t, \quad \forall g \in \mathcal{G}, t \in T \tag{6}$$

$$w_{\mathrm{BESS},t} = \frac{I^{\mathrm{sto,E}} e_s^{\mathrm{nom}} p_{\mathrm{BESS},t}^{\mathrm{dis}}}{E_{\mathrm{BESS}}^{\mathrm{lt}} \sqrt{\eta_{\mathrm{BESS}}^{\mathrm{rt}}}} = \frac{I^{\mathrm{sto,E}} p_{\mathrm{BESS},t}^{\mathrm{dis}}}{N_{\mathrm{BESS}}^{\mathrm{lt}} \sqrt{\eta_{\mathrm{BESS}}^{\mathrm{rt}}}}, \quad \forall t \in T \tag{7}$$

$$\begin{aligned} \mathrm{RC}_t = \beta^{\mathrm{R}} \Bigg[& \sum_{j \in J, j \neq \mathrm{pv}} \left(\Delta p_{j,t}^{\mathrm{SR+}} + \Delta p_{j,t}^{\mathrm{SR-}} + \Delta p_{j,t}^{\mathrm{S}} \right) \\ & + \Delta p_{\mathrm{BESS},t}^{\mathrm{SR+}} + \Delta p_{\mathrm{BESS},t}^{\mathrm{SR-}} + \Delta p_{\mathrm{BESS},t}^{\mathrm{S}} \Bigg], \quad \forall t \in T \end{aligned} \tag{8}$$

2.2 Components modeling

2.2.1 Photovoltaic (PV) system

The model that captures dependence of solar PV output power on both solar irradiance and ambient temperature is adapted from [30]. It also affects available power as long as cell temperature increases. Available solar photovoltaic power production is computed using the global horizontal irradiance (GHI) and assummed to be totally dispatched as PV power output as in Eq. (9) and cell temperature is computed with Eq. (10):

$$p_{\mathrm{pv,t}} = \eta_{pv} \frac{G_t}{G^{\mathrm{stc}}} \left[1 + \left(T_t^{\mathrm{mod}} - T^{\mathrm{stc}}\right) C_T\right] p_{pv}^{\mathrm{nom}}, \quad \forall t \in \mathcal{T} \tag{9}$$

$$T_t^{\mathrm{mod}} = T_t^{\mathrm{amb}} + G_t \left(\frac{T^{\mathrm{OpNom}} - 20}{800} \right), \quad \forall t \in \mathcal{T} \tag{10}$$

where G_t represents global horizontal irradiance (GHI); and G^{stc} and T^{stc} describe irradiance and temperature under standard conditions respectively. $C_T < 0$ is the PV temperature coefficient.

2.2.2 Chillers

Both absorption and electric chillers require an input energy source to generate cooling. An absorption chiller converts heat into cooling whereas an electric chiller turns electric power into cooling. Both cases are modeled in (11) and (12) respectively through performance coefficients as suggested in [31–33].

$$q_{\mathrm{ac},t} = \rho_{\mathrm{ac}} q_t^{ac,in}, \quad \forall t \in \mathcal{T} \tag{11}$$

$$q_{\mathrm{ec},t} = \rho_{\mathrm{ec}} q_t^{ec,in}, \quad \forall t \in \mathcal{T} \tag{12}$$

2.2.3 Energy storage systems

The state of charge (SOC) accounts for the amount of energy stored (kWh) in the system at time t. It is the result of continuous charging and discharging processes. SOC is shown in (13):

$$e_{s,t}^{\mathrm{SOC}} = (1 - \delta_s) e_{s,t-1}^{\mathrm{SOC}} + \left(\sqrt{\eta_s^{\mathrm{rt}}} p_{s,t}^{\mathrm{ch}} - \frac{p_{s,t}^{\mathrm{dis}}}{\sqrt{\eta_s^{\mathrm{rt}}}} \right) \Delta t, \forall S \in \mathcal{S}, \forall t \in \mathcal{T} \tag{13}$$

where η_s^{rt} is round-trip efficiency for storage system s. Also, $p_{s,t}^{\mathrm{dis}}, p_{s,t}^{\mathrm{ch}}$ is the discharge and charge power (in kW) for storage system s at time t, respectively. Parameter δ_s is the self-discharge rate and represents stored energy losses. The model presented in Eq. (13) applies for battery and thermal energy storage systems.

2.3 Operational constraints

2.3.1 Power balances

In each time step, electric power generated by generators needs to be either consumed by microgrid load or stored. The electric power balance is shown in constraint (14).

$$\sum_{j\in\mathcal{J}} p_{j,t} + p^{\text{dis}}_{\text{BESS},t} - D^{\text{el}}_t - p^{\text{ch}}_{\text{BESS},t} - \frac{q_{ec,t}}{\rho_{\text{ec}}} = 0, \forall t \in T. \tag{14}$$

Likewise, thermal energy produced by chillers needs to balance thermal load as shown in (15):

$$q_{\text{AC},t} + q_{\text{e},t} - Q^{\text{load}}_t = 0, \quad \forall t \in T. \tag{15}$$

The heat required by the heat load and the absorption chiller needs to be balanced by heat coming from TESS and thermal power plants as described in constraint (16). If any heat excess is generated, it might be wasted.

$$\sum_{j\in\mathcal{J}} \phi_j p_{j,t} + p^{\text{dis}}_{\text{TESS},t} - p^{\text{ch}}_{\text{TESS},t} - \frac{q_{ac,t}}{\rho_{\text{AC}}} - Q^{H-load}_t \geq 0, \ \forall t \in T. \tag{16}$$

2.3.2 Generation output constraints

Equations (17) and (18) ensure generation dispatch does not exceeds its nominal or minimum capacity. Binary variable $z_{j,t}$ decides whether or not to dispatch the power plant j at time t. Parameter M is a large scalar and guarantees that power plant j is limited by its nominal output only when it is dispatched, i.e., when $z_{j,t} = 1$.

$$p_{j,t} \geq \underline{\mu}_j p^{\text{nom}}_j - \left(1 - z_{j,t}\right)M, \quad \forall j \in \mathcal{J}, t \in T \tag{17}$$

$$p_{j,t} \leq \min\left(p^{\text{nom}}_j, z_{j,t} M\right), \quad \forall j \in \mathcal{J}, t \in T \tag{18}$$

2.3.3 Chillers output constraints

Constraints (19)-(20) ensure that chiller output is always between minimum and maximum operation point. Binary variable $z_{n,t}$ and M limit power output to its nominal value or zero if cooling resource is dispatched or not, respectively:

$$\underline{\mu}_n q^{nom}_n - (1 - z_{n,t})\, M \leq q_{n,t}, \quad \forall n \in N, t \in T \tag{19}$$

$$\min\left(q^{\text{nom}}_n, z_{n,t} M\right) \geq q_{n,t}, \quad \forall n \in N, t \in T \tag{20}$$

2.3.4 Storage constraints

Constraint (21) forces electricity and heat storage to be within specified minimum and maximum state-of-charge percentages. Constraints (22) and (23) bound instantaneous charge and discharge power output to nominal power output when scheduled; otherwise, charge/discharge is forced to be zero. Since p^{nom}_s is a decision

variable, Big-M constraint with binary decision is used. Binary decisions $z^{\text{ch}}_{s,t}$ and $z^{\text{dis}}_{s,t}$ prevent storage systems to charge and discharge simultaneously as constrained in Eq. (24):

$$\underline{\mu}^{\text{SOC}}_{s} e^{\text{nom}}_{s} \leq e^{\text{SOC}}_{s,t} \leq \bar{\mu}^{\text{SOC}}_{s} \cdot e^{\text{nom}}_{s}, \quad \forall s \in \mathcal{S}, t \in T \tag{21}$$

$$0 \leq p^{\text{ch}}_{s,t} \leq \min\left(p^{\text{nom}}_{s}, z^{\text{ch}}_{s,t} M\right), \quad \forall s \in \mathcal{S}, t \in T \tag{22}$$

$$0 \leq p^{\text{dis}}_{s,t} \leq \min\left(p^{\text{nom}}_{s}, z^{\text{dis}}_{s,t} M\right), \quad \forall s \in \mathcal{S}, t \in T \tag{23}$$

$$z^{\text{ch}}_{s,t} + z^{\text{dis}}_{s,t} \leq 1, \quad \forall s \in \mathcal{S}, t \in T \tag{24}$$

2.3.5 Ramp constraints

While some thermal generators, such as diesel generators, can respond from zero to full load in a much shorter time, ramp constraints may still apply to other types of generators with slower dynamics. In general, the proposed formulation allows for the possibility of including ramp constraints for any fuel-based generator. However, each case study will determine whether or not it is necessary to implement ramp constraints, which can be skipped setting the parameters r^{up}_{j} and r^{down}_{j} to 1. In the case of generators subject to ramp constraints, these constraints also limit the reserves allocation, ensuring that committed reserves can be depleted in the given time frame Δt. Rate of change of power output from fuel-fired generators is limited by maximum ramp to be loaded or downloaded. Equation (25) limits the rate of change from previous time-step to be within down and up ramp rates r^{down}_{j}, r^{up}_{j}, respectively [34]:

$$-r^{\text{down}}_{j} p^{\text{nom}}_{j} \leq \frac{p_{j,t} - p_{j,t-1}}{\Delta t} \leq r^{\text{up}}_{j} p^{\text{nom}}_{j} \quad \forall j \in \mathcal{J}, t \in T \tag{25}$$

2.4 Reliability constraints

Our approach guarantees reliable operation of the microgrid, i.e., microgrid components can "react" immediately to avoid load shedding once a contingency occurs. In this work, only electrical contingencies are taken into account. Thermal contingencies are not considered. To generalize the presentation of the model equations, all storage systems, including electric and thermal, were grouped together in a set called $\mathcal{S}$. The main operational constraints that limit stored energy and power output apply to every storage s, in these cases the general representation using the subscript s (e.g., $p^{\text{dis}}_{s,t}$) was used; however for exclusively electrical issues such as outages, only

electrical storage (*i.e., BESS*) is considered. Therefore, the subscript $(\cdot)_{\text{BESS},\ldots}$ for such constraints was used $\left(e.g., \Delta p^{s}_{\text{BESS},t}\right)$ considering that BESS $\in \mathcal{S}$.

2.4.1 $N-1$ reliability constraints

The proposed model forces a reliable operation under electric generation $N-1$ contingencies. When the contingency of the i-th element occurs, its power injection $p_{i,t}$ (or $p^{\text{dis}}_{\text{BESS},t}$ when the BESS fails) is lost. Except for the solar PV system, the remaining online generation must take over of lost power with the scheduled $N-1$ security reserve $\Delta p^{\text{S}}_{j,t}$ -$\Delta p^{\text{S}}_{\text{BESS},t}$ for BESS- supplying power to meet the demand and avoid load shedding. Therefore, generators and/or BESS power output should be ramped-up. For each time-step, a potential outage in each generator and electric storage is considered (i.e., a total of five different outages per hour are considered) and reliability reserves are scheduled. Each outage compromises both current power output and scheduled regulation reserve $\Delta p^{\text{SR+}}_{i,t}$, which need to be considered in the scheduling of reliability reserves. All of these aspects are carefully considered in constraints (26) and (27):

$$\sum_{j\in\mathcal{J}:j\neq i,j\neq pv} \Delta p^{\text{S}}_{j,t} + \Delta p^{\text{S}}_{\text{BESS},t} \geq p_{i,t} + \Delta p^{\text{SR+}}_{i,t}, \quad \forall t \in T, i \in \mathcal{J} \tag{26}$$

$$\sum_{j\in\mathcal{J}:j\neq pv} \Delta p^{\text{S}}_{j,t} \geq p^{\text{dis}}_{\text{BESS},t} + \Delta p^{\text{SR+}}_{\text{BESS},t}, \quad \forall t \in T \tag{27}$$

where $\Delta p^{\text{S}}_{j,t}$ and $\Delta p^{\text{S}}_{\text{BESS},t}$ are the allocated power reliability reserves in time-step t for generator j and BESS, respectively. $p_{i,t}$ and $\Delta p^{\text{SR+}}_{i,t}$ are lost power output from the outaged generator i and its allocated regulation reserve, respectively, that need to be supplied by all the remaining generators j-th.

2.4.2 Regulation reserves

Cloud cover, changes on irradiance patterns, and power demand fluctuations encourage the use of forecasting techniques for microgrid management. In addition to estimated $N-1$ reserves to face generation outages under $N-1$ criterion, the microgrid still needs to deal with both, solar PV and demand forecasting errors. The inherent random nature of these errors increase system regulation reserve requirements in order to balance generation and demand. Regulation reserves and (*i.e.,* spinning and non spinning reserves) are in charge to balance the system by adjusting the power output of generating units [35, 36]. In this work, a chance-constraint approach is proposed to allocate the regulation reserve to each generation based in the estimated regulation reserve requirements.

Several authors have explored the concept of defining a constraint to be met with a high probability, rather than as a conventional "hard" constraint with 100% certainty of satisfaction. However, our work adapts the foundations of chance-constrained optimization to the microgrid operational model. This adaptation is driven by the inherent uncertainties associated with solar generation and demand fluctuations in maintaining power balance. This has motivated us to propose a probability-based reserves allocation on top of the microgrid dispatch to maintain the generation-demand balance with a high probability. The interested reader can refer to [37] and [38] for additional material on chance constrained optimization.

Assuming the existence of hourly forecasts for electric power demand, D_t^{el} and solar PV generation, $p_{\text{pv},t}^{\text{av}}$, both actual random demand $\tilde{D}_t^{\text{el}}$ and random solar generation schedule $\tilde{p}_{\text{pv},t}$ can be expressed as (28) and (29) respectively:

$$\tilde{D}_t^{\text{el}} = D_t^{\text{el}} + \varepsilon_{D,t}, \quad \forall t \in \mathcal{T} \tag{28}$$

$$\tilde{p}_{\text{pv},t}^{\text{av}} = p_{\text{pv},t} + \varepsilon_{\text{pv},t}, \quad \forall t \in \mathcal{T} \tag{29}$$

where $\varepsilon_{D,t}$ and $\varepsilon_{\text{pv},t}$ represent hourly demand and solar PV estimation and forecast errors respectively, which are considered as independent random variables. The model so far has assumed that expected (or forecasted) demand can be met by both, forecasted solar PV and fuel-fired generation. However, random fluctuations in either demand or solar PV generation are not properly balanced in the model. Thus, it is essential to consider such random fluctuations on an hourly basis to properly scheduling regulation reserves.

Our approach is based on the idea of guaranteeing that electric demand can be satisfied with high probability. To do so, an amount of reserve is necessary to cover fluctuations of the net forecasting error ε_t defined as:

$$\varepsilon_t = \varepsilon_{D,t} - \varepsilon_{\text{pv},t}.$$

Net forecasting error can be either positive or negative, depending on the quality of forecasts. Net positive error requires additional generation; whereas net negative error requires a decrease in the generation to maintain demand-generation balance. As a result, in this approach, we distinguish the positive and negative parts of ε_t in order to schedule positive and negative regulation reserves. That is,

$$\varepsilon_t = \varepsilon_t^+ - \varepsilon_t^-$$

where $\varepsilon_t^+ = \max\left(\varepsilon_t, 0\right)$ and $\varepsilon_t^- = \max\left(-\varepsilon_t, 0\right)$. Therefore, we need to compute positive reserves SR_t^+ and negative reserves SR_t^- such that:

$$\mathbb{P}(\varepsilon_t^+ \leq \text{SR}_t^+) \geq 1 - \eta_t^+, \quad \forall t \in \mathcal{T} \tag{30}$$

$$\mathbb{P}(\varepsilon_t^- \leq \text{SR}_t^-) \geq 1 - \eta_t^-, \quad \forall t \in \mathcal{T} \tag{31}$$

According to the probabilistic criteria exposed in (30) and (31), deterministic regulation reserves SR_t^+ and SR_t^- guarantee that both, positive and negative imbalances will be covered with probability $1-\eta^+$ and $1-\eta^-$ or higher, respectively. In this sense, reserve amounts SR_t^+ need to be at least the $\left(1-\eta_t^+\right)$-th quantile $q_{t,1-\eta^+}^+$ of the probability distribution of ε_t^+. Likewise, and SR_t^- should be at least the $\left(1-\eta_t^-\right)$-th quantile $q_{t,1-\eta^-}^-$ of the probability distribution of ε_t^-:

$$\mathrm{SR}_t^+ \geq q_{t,1-\eta^+}^+, \quad \forall t \in T$$
$$\mathrm{SR}_t^- \geq q_{t,1-\eta^-}^-, \quad \forall t \in T.$$

Both quantiles, in general, can be computed from

$$q_{t,1-\eta^+}^+ = \begin{cases} q_{t,1-\eta^+}^{\varepsilon}, & \text{if } 1-\eta^+ \geq \mathbb{P}(\varepsilon_t < 0) \\ 0, & \text{otherwise,} \end{cases} \tag{32}$$

$$q_{t,1-\eta^-}^- = \begin{cases} -q_{t,\eta^-}^{\varepsilon}, & \text{if } 1-\eta^- \geq \mathbb{P}(\varepsilon_t > 0) \\ 0, & \text{otherwise.} \end{cases} \tag{33}$$

where $q_n^{\varepsilon} = F_{\varepsilon}^{-1}(n),\ n \in [0,1]$ refers to the n-th quantile of the distribution of the net forecast error ε; and $F_{\varepsilon}^{-1}(\cdot)$ is its corresponding inverse cumulative distribution function. An important feature of this formulation is that it can be employ with any probability distribution. Both $q_{t,1-\eta^+}^+$ and $q_{t,1-\eta^-}^-$ result in non-negative quantities.

When both errors are independent and normally distributed, i.e., $\varepsilon_{\mathrm{pv},t} \sim \mathcal{N}\left(\mu_{\mathrm{pv,t}}, \sigma_{\mathrm{pv},t}^2\right)$ and $\varepsilon_{D,t} \sim \mathcal{N}\left(\mu_{D,t}, \sigma_{D,t}^2\right)$, it is known for a fact that net error is also normally distributed. That is,

$$\varepsilon_t \sim \mathcal{N}\left(\mu_{D,t} - \mu_{\mathrm{pv,t}}, \sigma_{\mathrm{pv},t}^2 + \sigma_{D,t}^2\right), \quad \forall t \in T,$$

therefore, n-th quantile can be computed using (34), where $\mathrm{erf}^{-1}(n)$ is the inverse error function:

$$q_n^{\varepsilon} = \mu_{D,t} - \mu_{\mathrm{pv,t}} + \mathrm{erf}^{-1}(n)\sqrt{\sigma_{\mathrm{pv},t}^2 + \sigma_{D,t}^2}. \tag{34}$$

In the proposed approach, we assume that solar forecast error uncertainty is larger as long as solar production increases. In this sense, the hourly power output of the solar PV system ends up affecting parameters of the solar forecast error probability distribution. Solar PV mean forecast error $\mu_{\mathrm{pv,t}}$ and standard deviation $\sigma_{\mathrm{pv},t}$ are parameterized as percentages α_{pv} and ϑ_{pv} respectively of hourly scheduled PV power output $p_{\mathrm{pv},t}$. That is,

$$\mu_{\mathrm{pv,t}} = \alpha_{\mathrm{pv}} p_{\mathrm{pv},t}, \quad \forall t \in T$$
$$\sigma_{\mathrm{pv},t} = \vartheta_{\mathrm{pv}} p_{\mathrm{pv},t}, \quad \forall t \in T$$

Quantiles $q_{t,1-\eta^+}^+$ and $q_{t,1-\eta^-}^-$ that define the amount of positive and negative regulation reserves respectively are computed as follows:

$$q^{+}_{t,1-\eta^{+}} = \mu_{D,t} - \alpha_{\text{pv}} p_{\text{pv},t} + \text{erf}^{-1}(1-\eta^{+})\sqrt{\sigma^2_{D,t} + \vartheta^2_{\text{pv}} p^2_{\text{pv},t}}, \quad \forall t \in \mathcal{T} \tag{35}$$

$$q^{-}_{t,1-\eta^{-}} = \alpha_{\text{pv}} p_{\text{pv},t} - \mu_{D,t} - \text{erf}^{-1}(\eta^{-})\sqrt{\sigma^2_{D,t} + \vartheta^2_{\text{pv}} p^2_{\text{pv},t}}, \quad \forall t \in \mathcal{T} \tag{36}$$

Quantiles defined by Eqs. (35) and (36) represent the minimum amount of regulation reserves to schedule on an hourly basis. This formulation leads to the second-order cone nature of the proposed model. Additionally we do not impose that $q^{+}_{t,1-\eta^{+}}, q^{-}_{t,1-\eta^{-}} \geq 0$ in the model given the non-convexity of such constraints. Rather we verify that the optimal solution satisfies the non-negativity constraints on both quantiles. Finally, the positive and negative regulation reserve requirements are shown in (37) and (38) respectively, resulting in a set of conic constraints:

$$\sum_{j \in \mathcal{J}: j \neq pv} \Delta p^{\text{SR+}}_{j,t} + \Delta p^{\text{SR+}}_{\text{BESS},t} \geq q^{+}_{1-\eta^{+}_{t}}, \quad \forall t \in T, \tag{37}$$

$$\sum_{j \in \mathcal{J}: j \neq pv} \Delta p^{\text{SR}-}_{j,t} + \Delta p^{\text{SR-}}_{\text{BESS},t} \geq q^{-}_{1-\eta^{-}_{t}}, \quad \forall t \in T. \tag{38}$$

Both $N-1$ and positive regulation reserve requirements need to be high enough so as to meet the reliability constraints. However, reserves need to be tuned such that power output cannot exceed the nominal power of any generator as in (39); and are also bounded by maximum ramp-up power as in (40). For BESS, $N-1$ security reserve and up regulation reserves are limited by the current available energy stored and by its nominal power output as in (41).

$$p_{j,t} + \Delta p^{\text{SR+}}_{j,t} + \Delta p^{S}_{j,t} \leq p^{\text{nom}}_{j}, \forall j \in \mathcal{J} : j \neq \text{pv}, t \in T \tag{39}$$

$$\frac{\Delta p^{\text{SR+}}_{j,t} + \Delta p^{S}_{j,t} + p_{j,t} - p_{j,t-1}}{\Delta t} \leq r^{\text{up}}_{j} p^{\text{nom}}_{j}, \forall j \in \mathcal{J} : j \neq \text{pv}, t \in T. \tag{40}$$

$$\min\left(\frac{e^{\text{SOC}}_{\text{BESS},t} - \underline{\mu}^{\text{SOC}}_{\text{BESS}} e^{\text{nom}}_{\text{BESS}}}{\Delta t}, p^{\text{nom}}_{\text{BESS}} - p^{\text{dis}}_{\text{BESS},t}\right) \geq \Delta p^{\text{SR+}}_{\text{BESS},t} + \Delta p^{\text{S}}_{\text{BESS},t}, \forall t \in T \tag{41}$$

where $\Delta p^{\text{SR+}}_{j,t} \geq 0$, $\Delta p^{S}_{j,t} \geq 0$, $\Delta p^{\text{SR+}}_{\text{BESS},t} \geq 0$, and $\Delta p^{\text{S}}_{\text{BESS},t} \geq 0$ correspond to positive generator regulation reserve, generators $N-1$ security reserve, BESS up regulation reserves, and BESS $N-1$ security reserve, respectively.

Likewise regulation reserve constraints of power generation and BESS required to balance negative shifts in net forecasting error ε_t are shown in constraints (42)–(44):

$$p_{j,t} - \Delta p^{\text{SR}-}_{j,t} \geq \underline{\mu}_{j} p^{\text{nom}}_{j}, \forall j \in \mathcal{J} : j \neq \text{pv}, t \in T \tag{42}$$

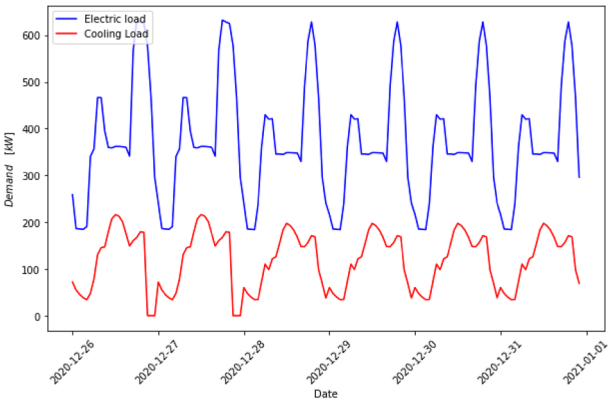

Fig. 2 Electric and thermal load patterns

$$\frac{p_{j,t-1} - p_{j,t} - \Delta p_{j,t}^{\mathrm{SR}-}}{\Delta t} \leq r_j^{\mathrm{down}} p_j^{\mathrm{nom}}, \forall j \in \mathcal{J} : j \neq \mathrm{pv}, t \in T \tag{43}$$

$$\Delta p_{\mathrm{BESS},t}^{\mathrm{SR}-} \leq \min\left(\frac{\bar{\mu}_{\mathrm{BESS}}^{\mathrm{SOC}} e_{\mathrm{BESS}}^{\mathrm{nom}} - e_{\mathrm{BESS},t}^{\mathrm{SOC}}}{\Delta t}, p_{\mathrm{BESS}}^{\mathrm{nom}} - p_{\mathrm{BESS},t}^{\mathrm{ch}}\right), \forall t \in T \tag{44}$$

where $\Delta p_{j,t}^{\mathrm{SR}-} \geq 0$ and $\Delta p_{\mathrm{BESS},t}^{\mathrm{SR}-} \geq 0$ correspond to negative generator and BESS regulation reserves, respectively. Down regulation reserves are bounded by both the minimum operational limit and the ramp-down limit for the generators. For the BESS, down regulation reserves are bounded by the available storage capacity without exceeding its maximum SOC limit, and by its nominal power input.

This regulation reserve approach allows to differentiate probabilities according to the needs of the microgrid. Violation probabilities η^+ and η^- must be small but can be different. Thus, it is possible to assign different small violation probabilities to either positive or negative imbalances. Additionally, probabilities can be different throughout the day. Also, any resulting probability distribution of forecast errors can be employed. In fact, even dependent random errors can be easily adapted to this formulation. Mitigating the proposed model conservativeness can be done by adjusting the maximum constraint violation probability $\eta_t^{(\cdot)}$. The larger this probability, the less conservative the solution. Constraints (37) and (38) allow to scheduling enough generation to face potential fluctuations (forecast errors) in demand and renewable generation as a function of the probability $\eta_t^{(\cdot)}$.

When implementing the explicit formulation of the scenarios, i.e. discretization of the model uncertainties, it results in a large-scale optimization problem with a reasonable number (maybe hundreds) of scenarios [38, 39]. Instead, the proposed computationally tractable chance-constrained has allowed to consider the continuous probability distribution of the combined (solar and demand) forecast error, which in turn permits the model user to set her/his own level of operational risk through the constraint violation probability. Also, despite the fact that the resulting second-order cone model is nonlinear (as opposed to the linear stochastic optimization version), it

Table 2 Microgrid component parameters

	PV	ICE	DSL	MT	EC	AC	BESS	TESS
$I_j^{\text{gen}}\left[\frac{\$}{\text{kW}}\right]$	1910	600	900	897	1350	1706	100	20
$I_s^{\text{sto,E}}\left[\frac{\$}{\text{kWh}}\right]$	0	0	0	0	0	0	580	75
$\pi_g\left[\frac{\$}{\text{MBTU}}\right]$	0	5.3	2.1	4.8	0	0	0	0
$a_g\left[\frac{\text{MBTU}}{\text{kWh}}\right]$	0	0.021	0.021	0.016	0	0	0	0
$b_g\left[\frac{\text{MBTU}}{\text{h}}\right]$	0	0	0	0	0	0	0	0
$\text{OM}_k^{\text{var}}\left[\frac{\$}{\text{kW}}\right]^*$	0	6	0	5.8	1	0	0	0
$\text{OM}_k^{\text{fix}}\left[\frac{\$}{\text{kW}}\right]^*$	1.47	0	0	0	0	0	1.6	0
$\text{ER}_k^{\text{CO}_2}\left[\frac{\text{kg}}{\text{kWh}}\right]$	0.04	0.18	0.25	0.18	0	0	0	0

*Values in $1e^{-3}$

is still convex. Furthermore, commercial solvers achieve global optimality as long as convexity is maintained in the model.

3 Case study

This section shows a case study to test the performance of the proposed model. We assume the resulting islanded microgrid will serve the facilities of a hotel in Cartagena, Colombia. The daily electric and thermal load profiles, on an hourly basis, are obtained from a large hotel facility in DER-CAM software [40] and are shown in Fig. 2. These patterns are split in weekdays and weekends. Peak electric demand is around 630 kW, whereas thermal demand is around 216 kW. Daily electric and thermal demands are 8900 kWh and 1700 kWh respectively. Since the hotel facility is

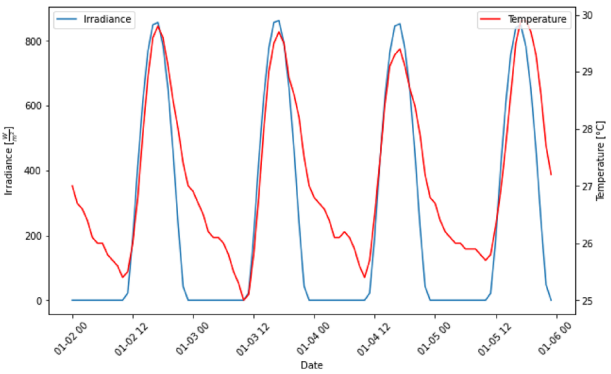

Fig. 3 Temperature and solar irradiance for the hotel

Table 3 Base case optimal microgrid sizing

Tech	Size [kW/kWh]	CAPEX [k$]	OPEX $\left[\frac{\text{k\$}}{\text{year}}\right]$	CO_2 [Ton]
PV	338.75	647.01	5.24	22.18
ICE	0.00	0.00	0.00	0.00
DSL	515.85	522.56	769.17	697.36
MT	0.00	0.00	0.00	0.00
BESS	150.24/654.50	394.63	22.37	0.00
TESS	0.00/0.00	0.00	0.00	0.00
HAC	0.00	0.00	0.00	0.00
EC	216.81	292.69	1.35	0.00
Total		1856.89	798.13	719.54

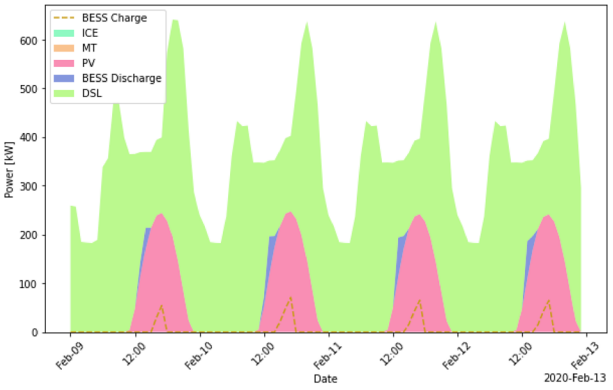

Fig. 4 Power output for microgrid technologies in base case

not expected to expand, energy demand levels are assumed as constant in the long term. Investment costs and emission rates are shown in Table 2. Emission rates for each technology are taken from [41] and [42]. The proposed formulation allows to account for the GHG emission for each kwh provided by the sized technology through the parameters $\text{ER}_k^{\text{CO}_2}$ and the emission tax cost ω_k. We have decided to account for the emissions of several technologies. Emissions from solar PV are also considered as indicated in [42], in which authors account for the life cycle emissions from the manufacture of solar cells. The CO_2 tax rate is 0.07 $\left[\frac{\$}{\text{kg}}\right]$ as suggested in [27].

The project lifespan is 15 years. This case study considers $|\mathcal{T}| = 8760$ hourly periods in order to represent the entire microgrid operations in the sizing problem. This implies $\gamma = 1$. An interest rate of 6% is employed to discount future cash flows. Up and down regulation reserve cost β^R is set as 40% of the degradation cost of battery storage as in [21]. The average cycles to failure $N_{\text{BESS}}^{\text{lt}}$ is set to 995 (computed using data from [28]). Solar and electric load estimation error $\tilde{\varepsilon}_{pv,t}$, $\tilde{\varepsilon}_{D,t}$ are assumed to be

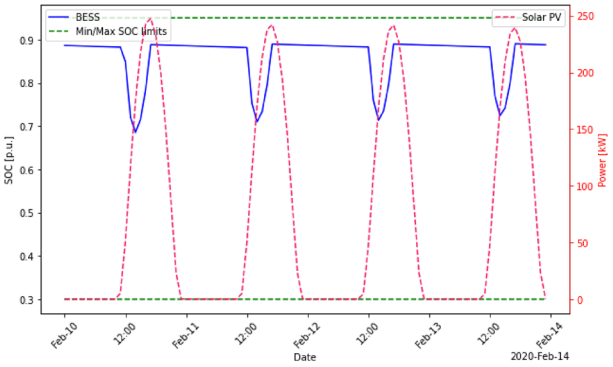

Fig. 5 State-of-charge for ESS in base case

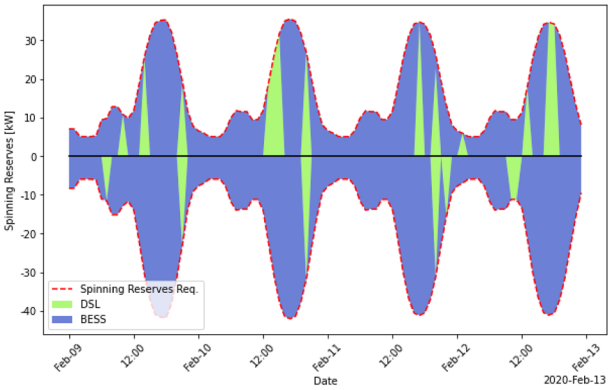

Fig. 6 Up and down reserves requirements due intermittency in basecase

normally distributed $\mathcal{N}_{\epsilon_{pv}}\left(\mu_{pv,t} = \alpha_{pv} p_{pv,t}, \sigma_{pv,t} = \vartheta_{pv} p_{pv,t}\right)$, with $\alpha_{pv} = 0$ and $\vartheta_{pv} = 0.1$ and $\mathcal{N}_{\epsilon_D}\left(\mu_{D,t} = 0, \sigma_{D,t} = 0.02 D_t^{el}\right)$, respectively. The allowable violation probabilities of regulation reserves are set as $\eta^- = \eta^+ = 0.05$. Meteorological parameters of Cartagena are displayed in Fig. 3. Temperature data have been taken from IDEAM [43] and solar irradiance from Solcast [44]. The model is implemented in `Pyomo 5.7.3` [45] and solved using `Gurobi 9.5.0` [46] executed on an intel Core i7-8700 with 16GB RAM.

4 Results

4.1 Base case

In the base case, only up and down regulation reserves are considered. Security reserves due to sudden outages are ignored in this case. The optimal sizing, CAPEX,

annual OPEX and annual CO_2 emissions for each technology in the base case are shown in Table 3. Diesel-generator, PV and BESS are selected for supplying electric power, while an electric chiller (EC) supplies the thermal energy demand. The objective function adds up to $10.3 million. Although the operational commitment is considered during 8760 hly periods, only the first four days are displayed in Fig. 4. Despite the relative high OPEX of diesel generation, it is heavily scheduled as the main generator to meet electric load. During peak sunlight hours, PV supplies a significant share of load and BESS charge. The remaining load is supplied mainly by the diesel generator. BESS discharge also provides support during the peak-hours.

The state-of-charge (SOC) of BESS is shown in Fig. 5. BESS is scheduled to be charged (upward SOC) mainly during peak sunlight hours with PV system. Discharge (downward SOC) is scheduled during both, the mornings and peak load hours under absence of solar PV production.

Base case optimal up and down regulation reserves allocation and requirements on the base case are depicted in Fig. 6. This case ignores $N-1$ reserves and only regulation reserves are imposed. The size of the requirements depends on the probability distribution of net forecast error (difference between both electric load and PV system forecast errors). For the PV system, the larger the scheduled PV output, the larger reserve would be needed. DSL and BESS are the only dispatchable resources installed in this case (MT and ICE are not installed). As a result, regulation reserve requirements are covered mainly by BESS. That is, BESS would face potential intermittencies given the non-dispatchability and potential high forecast error of the PV-system production. Stored energy acts as an up-regulation reserve to cover sudden net load increments or any potential renewable intermittency; down-regulation reserve is employed to store a sudden surge of energy. Considering degradation wear costs leads to the use of BESS mainly as a reserve provider. Scheduling BESS for energy provision accelerates discharge cycles, which is represented in capacity loss and higher replacement costs.

In this case, thermal load is always supplied by EC. MT and ICE, providers of recovered heat, are of no interest to the model given their high operational and investment cost. This, in turn, yields the model to not install any AC. As a result, TESS is not necessary in the optimal microgrid design.

Table 4 Sizing results for reliability-based design

Tech	Size [kW/kWh]	CAPEX [k$]	OPEX $\left[\frac{\text{k\$}}{\text{year}}\right]$	CO_2 [Ton]
PV	325.75	622.18	5.04	21.33
ICE	18.63	11.18	47.30	8.92
DSL	320.14	324.31	492.99	454.54
MT	320.14	287.17	659.72	163.09
BESS	318.02/489.55	315.74	36.84	0.00
TESS	40.29/226.12	17.76	0.00	0.00
HAC	63.20	107.82	0.00	0.00
EC	153.61	207.37	0.89	0.00
Total		1893.53	1242.76	647.88

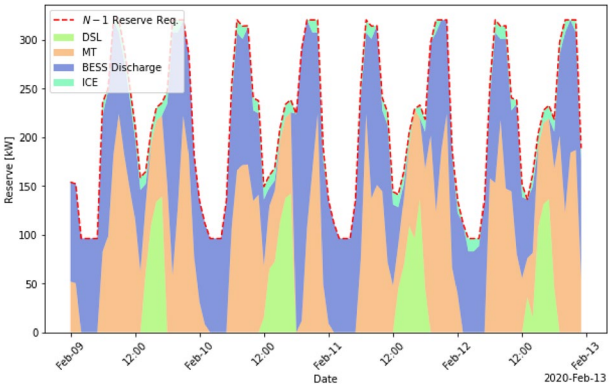

Fig. 7 Reserve schedules for $N-1$ contingencies in the reliability-based case

4.2 Reliability-based microgrid design

4.2.1 Numerical results

The Reliability-based design includes all constraints presented in the proposed model in Sect. 2. Sizing, CAPEX, annual OPEX, and annual CO_2 emissions for each technology in the microgrid are shown in Table 4. The total objective function is \$16.5 millions. The energy mix is more diversified than the base case to avoid high dependency on a specific technology. PV system is the largest generator, closely followed by DSL, MT and ICE. The BESS capacity is sized to be discharged in approximately an hour and a half at its nominal power output. Although conventional fuel-fired generation represents a larger share than renewable resources, CO_2 emissions are reduced compared to the base case.

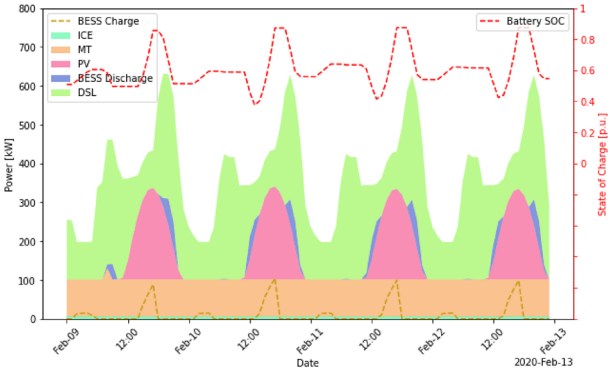

Fig. 8 Power output for microgrid technologies with reliability-based design

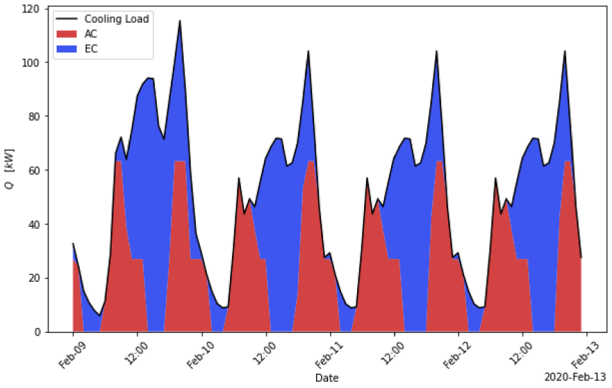

Fig. 9 Thermal load and chillers output

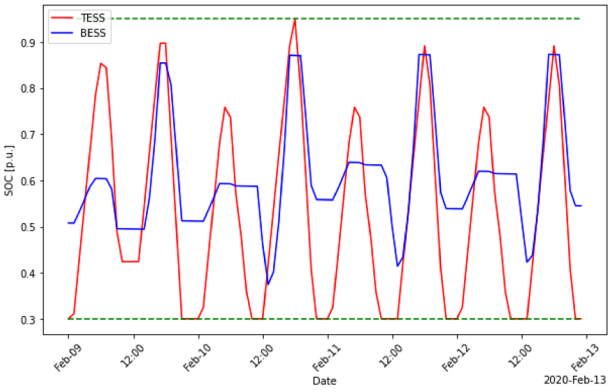

Fig. 10 State-of-charge for ESS in reliability-based design

The provision reserves against $N-1$ contingencies on for the reliability-based design case are shown in Fig. 7. $N-1$ reserves requirements avoid any generator to supply the entire electric load; rather, all generators are scheduled to a moderate power output. The model allocates reserves for each dispatchable technology such that, for any sudden generator loss at any hour, the microgrid has enough mix of $N-1$ reserves. Once a generator is faulted, $N-1$ reserves, provided by remaining generators, should be enough to continuously satisfy electric demand. The proposed approach in this work diversifies both energy provision and reserve allocation by avoiding a single generator providing all of the reserve and energy requirements. Required reserves are determined by the largest generator's output plus the largest allocated regulation reserve per period. Thus, this balance between operating efficiency and reserve capacity entails a trade-off: increasing generation capacity

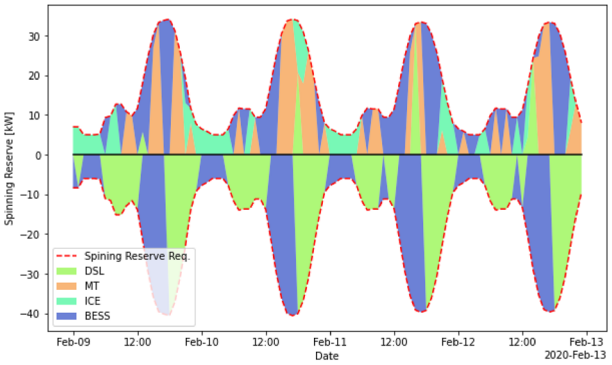

Fig. 11 Up and down regulation reserves requirements in reliability-based design

Table 5 Optimization problem characteristics

	Base case	Reliability-based case
Time [min]	25.98	42.6
Constraints	623,666	676,370
Conic constraints	17,568	17,568
Variables	351,372	351,372
Binary Vars	87,840	87,840
Obj. Func. [$]	10,303,246	16,556,278

enhances efficiency; however, it also increases the need for $N-1$ reserve, which in turn imposes generators to operate at lower power output levels

As shown in the operational scheduling in Fig. 8, MT and ICE are continuously dispatched at its minimum operative output, whereas DSL supplies the remaining load. During sunlight hours, solar PV power is employed to charge the BESS and supply a fraction of load, which eventually reduces DSL production. Thus, MT and BESS are the main reserve providers against contingencies. When PV production is high, DSL is enabled to provide reserves in case of an outage. As a result of the reliable operation of the microgrid, operational cost tends to be high given the significant use of conventional fuel-fired generation.

Figure 9 displays the schedule of thermal systems. Unlike the base case results, the AC takes advantage of the heat recovered from the burnt fuel of MT and ICE to provide cooling. Remaining thermal demand is supplied by the EC, which in turn imposes an additional electric load to the microgrid. Several hours before the peak-cooling load condition, recovered heat from MT and ICE is not employed by the AC, but stored in the TESS. Once in peak-cooling load condition, the TESS provides heat to the AC, which delivers energy to thermal loads in order to reduce the EC participation.

The state-of-charge for each storage system is shown in Fig. 10. BESS is charged by the PV-system and by the fuel-fired generator when solar production vanishes and electric load is the lowest. BESS is discharged during peak-load

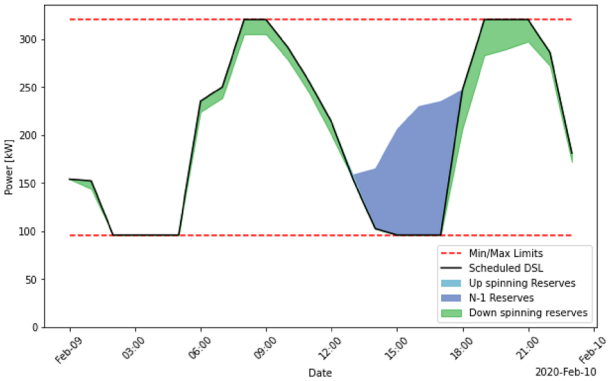

Fig. 12 Diesel generator scheduled output and reserves

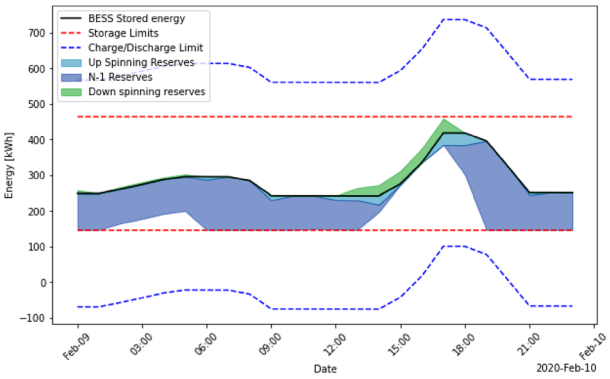

Fig. 13 BESS Stored energy and scheduled reserves

hours and during the night-hours when PV is zero. Since BESS is also scheduled as reserve provider, it is rarely fully discharged.

Reserves for intermittency are splitted in up/down regulation reserves as displayed by dashed lines in Fig. 11. Up regulation reserves are covered by almost all technologies online, which are available to be ramped-up to deal with either random intermittencies in PV output or changes in electric load. Down reserves are intended to decrease power production (or store any energy surplus in the BESS) given an increase in PV-power output or decrease in load demand. Down regulation reserve requirements are covered mainly by DSL, which is scheduled close to its rated power. BESS also provides down reserves when its SOC is low. MT and ICE do not offer down reserves since they are scheduled at their minimum levels.

For both the base case and the reliability-based case, the info of CPU time, number of constraints, number of conic constraints, number of variables, number of binary variables and objective function values are shown in Table 5. The CPU time for the full reliability-based case is close to 42 min.

4.2.2 Reserve requirements

Regulation and $N-1$ security reserves, impose requirements to power output in generators and BESS. $N-1$ and up regulation reserve require the generator power output and BESS discharging to be ready to increase if needed; on the other hand, down regulation reserves require the generator and BESS discharging to be reduce if needed. For the BESS, reserves are scheduled to take advantage of its ability to absorb energy in the charging mode. Figures 12 and 13 depict the scheduled power output, up/down regulation reserves allocation and $N-1$ security reserves for DSL and BESS respectively. Both allocated reserves are scheduled based on the excess generator capacity, without exceeding their nominal or ramp limits. In the case of DSL, the output limits are imposed by the nominal power output and maximum up/down ramps. DSL schedules down regulation reserves without exceeding the minimum operational value. Likewise, $N-1$ and up regulation reserves are rigorously scheduled avoiding producing power above nominal values of generation resources.

Despite the fact that BESS reserves are limited by available stored energy and nominal charge/discharge power output, the optimal sizing shows that BESS is a significant reserve provider. For $N-1$ reserves, BESS is scheduled to increase its power output (discharging mode). The $N-1$ reserve provision is high when either its SOC is at medium/high levels or BESS is already discharging due to the absence of sunlight and PV output. For down regulation reserves, BESS reserves are scheduled when sunlight is at peak. If any deviation occurs, the BESS may reduce its power output and even absorb any energy excess (charging mode) to cover the demand/PV forecasting deviation. Equation (8) offers a general formulation that allows reserve costs to be allocated as proposed in the literature [21]. However, the reserve cost could be set to zero if needed. After running the model setting reserve cost to zero, the impact on the optimal microgrid sizing is negligible; but, the scheduling of regulation reserves increases. The model schedules up(down) regulation reserves beyond the computed requirements due to lack of reserve cost. Remaining available power (scheduled output above minimum) is allocated as up(down)

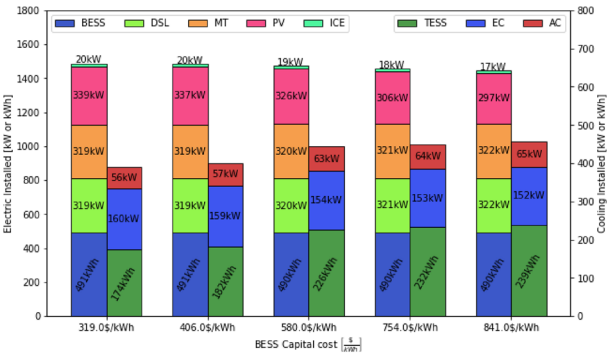

Fig. 14 Optimal microgrid sizing vs BESS investment cost

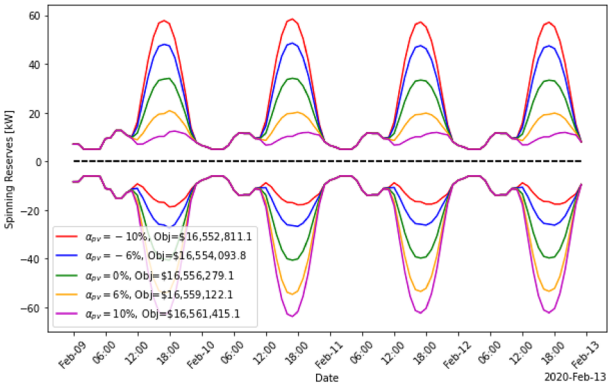

Fig. 15 Up and down regulation reserve requirements under changes in α_{pv}

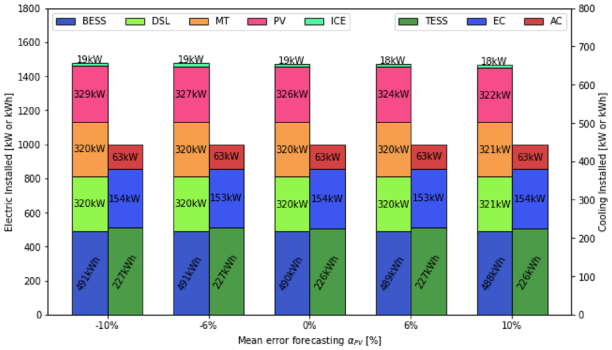

Fig. 16 Optimal microgrid sizing vs changes in the the solar mean forecast error α_{pv}

regulation reserves. This in turn implies additional $N-1$ reserves that need to be provided to deal with potential outages

4.3 Sensitivity analysis

4.3.1 Sensitivity analysis for investment cost

To comprehensively evaluate the performance of the proposed model under different circumstances, a sensitivity analysis in BESS capacity investment cost is carried out. To analyze the impact of BESS investment cost $\left(I_{\text{BESS}}^{\text{sto,E}}\right)$ on technology sizing, variations between 70% and 130% of the its nominal value (580 $/kWh) were considered. Figure 14 shows that higher investment cost per kW does not cause significant changes in the BESS installed capacity. The main change in the analysis is the amount of energy discharged from the BESS. For the lowest value (319 $/kWh) 996,961 kWh are discharged; whereas the case with the highest value (841 $/kWh),

only 423,975 kWh are discharged annually from the BESS. This condition stems from the BESS investment cost, which heavily affects the wear cost. If it is low, then BESS participation is high. On the contrary, the wear cost tends to be excessively high and the BESS only participates as reserve provider. Also, MT and DSL nominal capacities barely change; but are constantly scheduled to operate, which would recover additional heat. As a result, the sizing of AC and TESS is such that it can take advantage of the increased heat and thus reduce the EC participation. The simultaneous occurrence of peaks in both electric and thermal load forces the model to employ more AC (which is fed by heat stored in the TESS and recovered heat from MT and ICE) than EC. The objective function ranges from $16.5 millions (319 $/kWh) to $16.8 millions (841 $/kWh).

4.3.2 Sensitivity analysis with respect to solar forecast error

The net error distribution of solar production and electric load directly affects the regulation reserve requirements. Figure 15 depicts the reserve requirements for up and down regulation reserves under changes in the error mean of the solar production forecast $\mu_{pv,t}$, while Fig. 16 shows the optimal microgrid sizing in each case. Negative solar mean forecast error (forecast overestimates actual production) increases the up regulation reserves and reduce down reserves. For large negative mean errors, PV system size increases and fuel-fired production decreases, which causes a decrease in the objective function. Large positive mean error forecast decreases up regulation reserves and increases down regulation reserve requirements. Unlike up regulation reserves, down reserves are supported mainly by BESS

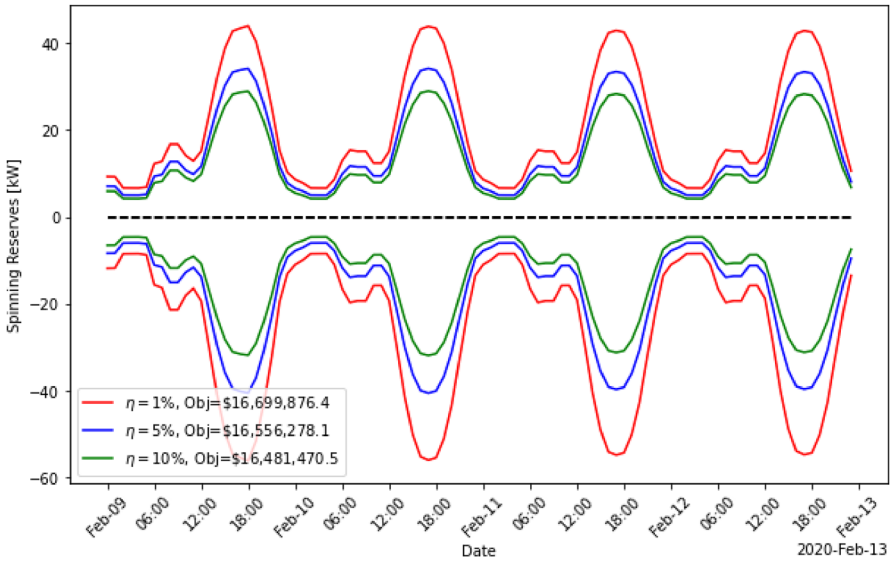

Fig. 17 Up and down regulation reserve requirements under changes in η

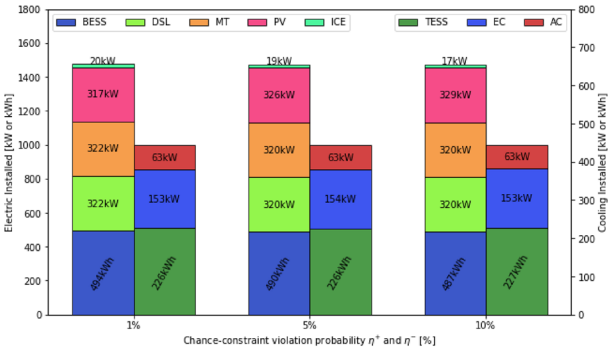

Fig. 18 Optimal microgrid sizing vs probabilities η^+ and η^-

and DSL (MT and ICE are dispatched at their operational minimum.) To face increasing down regulation reserve requirements, the model reduces the PV system size and increases DSL schedule to extend the amount of down regulation reserve available in DSL. Non-negativity conditions for quantiles in Eqs. (35) and (36) are verified on an hourly basis. Even for extreme values, $\alpha_{\text{pv}} = \pm 10\%$ quantiles are still non negative.

4.3.3 Sensitivity analysis with respect to regulation reserve violation probabilities

According to the probabilistic criteria exposed in Eqs. (30) and (31), the model imposes that scheduled regulation reserve requirements should cover positive and negative imbalances in demand-generation with probabilities at least $1 - \eta^+$ and $1 - \eta^-$ respectively. The reserve commitment of the proposed model and its implications is analyzed in this part via the following three cases:

- Reference case: $\eta^+ = \eta^- = 0.05$.
- High probability case: $\eta^+ = \eta^- = 0.10$.
- Low probability case: $\eta^+ = \eta^- = 0.01$.

Figure 17 shows variation of up and down regulation reserve requirements in a short time span when forecast mean errors are zero ($\mu_{\text{D},t} = \mu_{\text{pv},t} = 0$). And Fig. 18 shows the optimal microgrid design in each case. As expected, the lower probabilities η^+ and η^-, the higher up and down regulation reserve requirements. To schedule high regulation reserves, conventional fuel-fired generators and BESS are high-sized. As the probabilities η^+ and η^- increase, solar PV participation increases, which reduces operational expenditures. Also, non-negativity conditions stated in Eqs. (35) and (36) always hold.

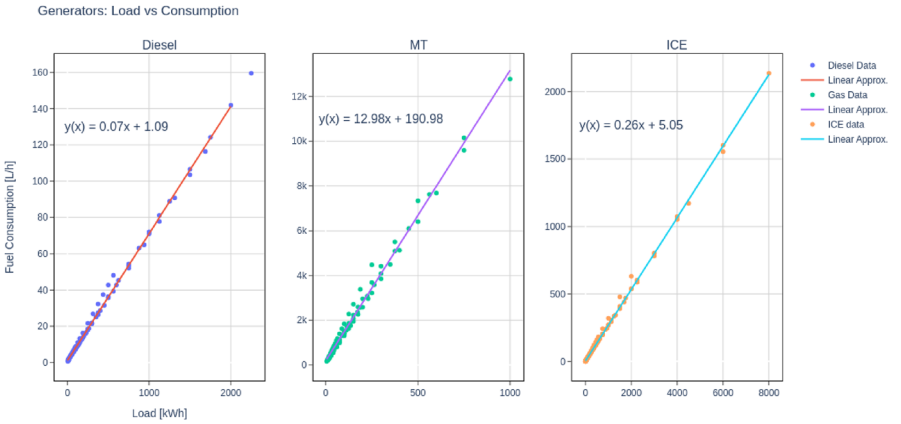

Fig. 19 Linear approximation of fuel consumption

Table 6 Sizing results for industrial parameters a_g and b_g

Tech	Size [kW/kWh]	CAPEX [k$]	OPEX $\left[\frac{\text{k\$}}{\text{year}}\right]$	CO_2 [Ton]
PV	199.38	380.81	3.08	13.05
ICE	267.63	160.58	258.09	139.39
DSL	0.00	0.00	0.00	0.00
MT	386.87	347.02	141.73	386.81
BESS	386.87/595.55	384.11	13.73	0.00
TESS	27.69/130.80	10.36	0.00	0.00
HAC	104.94	179.04	0.00	0.00
EC	111.87	151.02	0.32	0.00
Total		1612.94	416.95	539.25

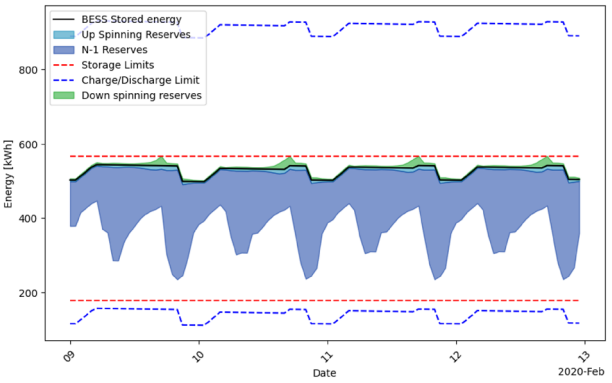

Fig. 20 BESS schedule Output, $N-1$ reserves, regulation reserves with modified fuel-consumption parameters

Table 7 Sizing results for reliability-based study with no wear cost

Tech	Size [kW/kWh]	CAPEX [k$]	OPEX $\left[\frac{\text{k\$}}{\text{year}}\right]$	CO_2 [Ton]
PV	316.97	605.42	4.90	20.75
ICE	0.00	0.00	0.00	0.00
DSL	350.26	354.81	517.08	466.30
MT	344.09	308.65	676.29	167.19
BESS	317.35/493.71	7.18	86.14	0.00
TESS	8.52/35.17	2.81	0.00	0.00
HAC	34.82	59.40	0.00	0.00
EC	181.99	245.69	10.78	0.00
Total		1894.87	1206.36	654.23

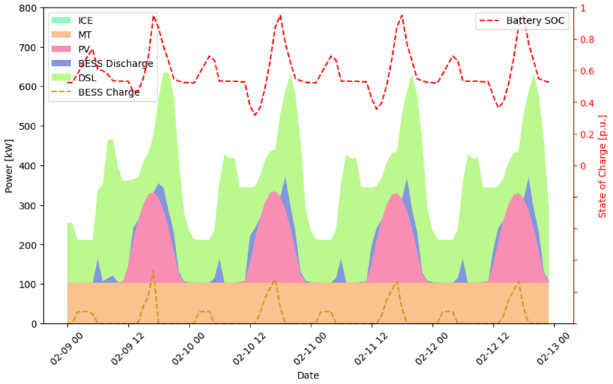

Fig. 21 Power output for technologies in the reliability-based case with no BESS wear cost

4.3.4 Fuel-consumption curve parameters

In this section, we present a comprehensive analysis of the fuel-consumption parameters a_g and b_g in the proposed formulation and their impact on both the sizing and operational aspects of the reliability-based study case under consideration. A new case based in the reliability case in Sect. 4.2 is proposed, where parameters a_g and b_g for each generator type were approximated from industrial data. Parameters a_g and b_g for each generator type were approximated from industrial data. Specifically, for Diesel Fuel Consumption [47], Natural Gas Consumption [48] and, ICE fuel consumption [12]. the data was fitted to a straight line as shown in Fig. 19 and converted to MBTU using average heat content from [49]. Results are presented in Table 6.

The DSL generator is not selected as part of the energy mix due to its high operating costs. Fuel consumption and the high price of diesel make it uneconomical to use the generator. To replace the power supplied by DSL, both ICE and the MT increase their rated power and are scheduled with a higher output at each timestep. Due to the amount of heat available to be recovered from the ICE and MT, the HAC increases its capacity while the participation of the EC decreases. Because now only

two fuel-fired generators provide most of the required power with a higher output, the $N-1$ reserve requirements are higher and provided mainly by the BESS. BESS cycling policy is now set as reserve provider to allows the reserve requirement to be met and avoid MT to run at low power output. This behaviour is depicted in Fig. 20. In contrast to the reliability-based case, in this case the consumption and cost of diesel fuel is much higher. Therefore, the model decided not to use the DSL generator, not even as reserves provider, as it is very expensive to keep it running to provide reserves due to fuel consumption.

4.3.5 BESS wear cost

This section presents an analysis of the BESS wear cost $\omega_{\text{BESS},t}$ related to microgrid sizing. This cost of accounts for the BESS degradation due to cycling energy through the storage system. It quantifies the cumulative degradation incurred by each kWh provided by the battery until its lifetime energy throughput is depleted. Equation (7) incorporates the BESS wear cost approach in the objective function, which affects BESS cycling. As a result, the optimal cycling policy is based on a trade-off among generator fuel cost, generators fuel consumption, battery wear cost and reserve requirements. A full reliability-based case without BESS wear cost is performed and the corresponding results are presented in Table 7.

The main changes comparing this case with respect to the reliability-based case presented in Sect. 4.2 is the lack of ICE generator in the sized mix. The ICE power is replaced with a higher rated power to DSL, MT and BESS. Since no heat is recovered from ICE, HAC and TESS are significantly reduced. The power scheduling is depicted in Fig. 21. In this case, BESS is cycled more often at lowest SOC w.r.t. the reference case. The BESS power output is higher and more recurrent while still providing regulation and $N-1$ reserves because no degradation is considered. Since the remaining generators provide higher power output and regulation reserves to replace the ICE, the $N-1$ reserve requirement are increased to cover any potential outage in the sized generators.

5 Conclusions

This paper presents a novel reliability-based methodology to optimally design an isolated microgrid with both electric and thermal demands. The optimal design covers technology selection and sizing from a distributed energy resources portfolio. The interplay between thermal and electricity flows with the microgrid were effectively considered via linear constraints. To provide a reliable design and operation, a set of constraints against sudden $N-1$ generation contingencies was proposed. Also, a high percentage of random fluctuations of demand and/or intermittent generation were handled by a set of probabilistic chance-constraints that determine minimum amounts of hourly regulation reserves. This type of constraints determined the second-order conic nature of the mathematical model.

When reliability constraints are included in the model, the participation of dispatchable resources in the optimal design of the microgrid increases as a result of higher reserve requirements; but, renewable technologies participation decreases. As a result, not only larger nominal power capacities are installed, but also higher operational expenditures are observed given the significant costly production of fuel-fired technologies.

Reliance on few generation projects leads to high $N-1$ reserve requirements to mitigate the risk of generator outages. Meeting these reserve requirements with conventional generators increases fuel costs as the generators must reduce their power output to provide reserves, which leads to partially loaded fuel-fired generator and increased fuel consumption

BESS-capacity investment cost is a key parameter in the BESS operations. As long as such a cost is reduced, BESS is heavily scheduled; otherwise, BESS capacity barely changes and is mainly employed for reserves provision. This in turn increases the participation of the fuel-fired technologies, absorption chiller, and thermal storage system.

The wear cost $\omega_{\mathrm{BESS},t}$, accounting for energy cycling through the BESS is used to effectively assess battery capacity degradation. The BESS cycling policy is optimally determined based on a trade-off between fuel costs and wear cost in order to reduce CAPEX and OPEX.

Finally, in order to avoid the typical zero-mean assumptions of random forecast errors, our chance-constraints carefully differentiate positive from negative errors. Forecast errors are not necessarily unbiased, as in real life. While a positive error mean increases down-regulation reserves (and reduces up reserves), a negative error mean increases up-regulation reserves (and reduces down reserves). However, the effect of imposing low violation probability of handling random forecast errors always translates into high up- and down-regulation reserves.

Acknowledgements This research was funded by Celsia Colombia S.A. E.S.P. and was awarded by Minciencias under Grant 786-2019 (code 8101-786-65958).

Author Contributions Juan C. Camargo-Berrueco: investigation, validation, writing—original draft, writing—review and editing, software. Diego Mejía-Giraldo: conceptualization, formal analysis, validation, writing—review and editing, methodology. Santiago Lemos-Cano: conceptualization, supervision, resources, funding acquisition.

Funding Open Access funding provided by Colombia Consortium.

Data availability Datasets related to this article can be found at https://github.com/pybegginer/microgrid_sizing hosted at Github.

Declarations

Conflict of interest The authors declare that they have no known competing financial or personal relationships that could have appeared to the work reported in this paper.

References

1. Hossain, E., Kabalci, E., Bayindir, R., Perez, R.: Microgrid testbeds around the world: state of art. Energy Convers. Manag. **86**, 132–153 (2014). https://doi.org/10.1016/j.enconman.2014.05.012
2. IRENA: Renewable power generation cost in 2019. Technical report, IRENA, Abu Dhabi (2020)
3. IRENA: Innovation Outlook: Renewable Mini-Grids. Technical report, IRENA, Abu Dhabi (2016)
4. Scioletti, M.S., Newman, A.M., Goodman, J.K., Zolan, A.J., Leyffer, S.: Optimal design and dispatch of a system of diesel generators, photovoltaics and batteries for remote locations. Optim. Eng. **18**(3), 755–792 (2017). https://doi.org/10.1007/s11081-017-9355-4
5. Barry, N.G., Santoso, S.: Military diesel microgrids: design, operational challenges, energy storage integration. In: 2021 IEEE Power and Energy Society General Meeting (PESGM), pp. 1–5 (2021). https://doi.org/10.1109/PESGM46819.2021.9637999
6. Menon, R.P., Paolone, M., Maréchal, F.: Study of optimal design of polygeneration systems in optimal control strategies. Energy **55**, 134–141 (2013). https://doi.org/10.1016/j.energy.2013.03.070
7. Nikolaidis, P., Chatzis, S., Poullikkas, A.: Optimal planning of electricity storage to minimize operating reserve requirements in an isolated island grid. Energy Syst. **11**(4), 1157–1174 (2019). https://doi.org/10.1007/s12667-019-00355-x
8. Mishra, S., Pohl, J., Laws, N., Cutler, D., Kwasnik, T., Becker, W., Zolan, A., Anderson, K., Olis, D., Elgqvist, E.: Computational framework for behind-the-meter DER techno-economic modeling and optimization: REopt lite. Energy Syst. **13**(2), 509–537 (2021). https://doi.org/10.1007/s12667-021-00446-8
9. Hirwa, J., Ogunmodede, O., Zolan, A., Newman, A.M.: Optimizing design and dispatch of a renewable energy system with combined heat and power. Optim. Eng. **23**(3), 1–31 (2022). https://doi.org/10.1007/s11081-021-09674-4. (**Cited by: 9; All Open Access, Green Open Access**)
10. Petrelli, M., Fioriti, D., Berizzi, A., Poli, D.: Multi-year planning of a rural microgrid considering storage degradation. IEEE Trans. Power Syst. **36**(2), 1459–1469 (2021). https://doi.org/10.1109/TPWRS.2020.3020219
11. Carvallo, C., Jalil-Vega, F., Moreno, R.: A multi-energy multi-microgrid system planning model for decarbonisation and decontamination of isolated systems. Appl. Energy **343**, 121143 (2023). https://doi.org/10.1016/j.apenergy.2023.121143
12. Moretti, L., Astolfi, M., Vergara, C., Macchi, E., Pérez-Arriaga, J.I., Manzolini, G.: A design and dispatch optimization algorithm based on mixed integer linear programming for rural electrification. Appl. Energy **233–234**, 1104–1121 (2019). https://doi.org/10.1016/j.apenergy.2018.09.194
13. Li, B., Roche, R., Miraoui, A.: Microgrid sizing with combined evolutionary algorithm and MILP unit commitment. Appl. Energy **188**, 547–562 (2017). https://doi.org/10.1016/j.apenergy.2016.12.038
14. Li, B., Roche, R., Paire, D., Miraoui, A.: Sizing of a stand-alone microgrid considering electric power, cooling/heating, hydrogen loads and hydrogen storage degradation. Appl. Energy **205**(September), 1244–1259 (2017). https://doi.org/10.1016/j.apenergy.2017.08.142
15. Dakir, S., Boukas, I., Lemort, V., Cornélusse, B.: Sizing and operation of an isolated microgrid with building thermal dynamics and cold storage. In: 2019 IEEE International Conference on Environment and Electrical Engineering and 2019 IEEE Industrial and Commercial Power Systems Europe (EEEIC/I CPS Europe), pp. 1–6 (2019). https://doi.org/10.1109/EEEIC.2019.8783514
16. Dakir, S., Boukas, I., Lemort, V., Cornélusse, B.: Sizing and operation of an isolated microgrid with cold storage. In: 2019 IEEE Milan PowerTech, pp. 1–6 (2019). https://doi.org/10.1109/PTC.2019.8810700
17. Dakir, S., Boukas, I., Lemort, V., Cornélusse, B.: Sizing and operation of an isolated microgrid with building thermal dynamics and cold storage. IEEE Trans. Ind. Appl. **56**(5), 5375–5384 (2020). https://doi.org/10.1109/TIA.2020.3005370

18. Mashayekh, S., Stadler, M., Cardoso, G., Heleno, M.: A mixed integer linear programming approach for optimal DER portfolio, sizing, and placement in multi-energy microgrids. Appl. Energy **187**, 154–168 (2017). https://doi.org/10.1016/j.apenergy.2016.11.020
19. Micangeli, A., Fioriti, D., Cherubini, P., Duenas-Martinez, P.: Optimal design of isolated minigrids with deterministic methods: matching predictive operating strategies with low computational requirements. Energies **13**(6) (2020). https://doi.org/10.3390/en13164214
20. Wang, M.Q., Gooi, H.B.: Spinning reserve estimation in microgrids. IEEE Trans. Power Syst. **26**(3), 1164–1174 (2011). https://doi.org/10.1109/TPWRS.2010.2100414
21. Liu, G., Starke, M., Xiao, B., Zhang, X., Tomsovic, K.: Microgrid optimal scheduling with chance-constrained islanding capability. Electr. Power Syst. Res. **145**, 197–206 (2017). https://doi.org/10.1016/j.epsr.2017.01.014
22. Sefidgar-Dezfouli, A., Joorabian, M., Mashhour, E.: A multiple chance-constrained model for optimal scheduling of microgrids considering normal and emergency operation. Int. J. Electr. Power Energy Syst. **112**, 370–380 (2019). https://doi.org/10.1016/j.ijepes.2019.05.026
23. Hemmati, M., Mohammadi-Ivatloo, B., Abapour, M., Anvari-Moghaddam, A.: Optimal chance-constrained scheduling of reconfigurable microgrids considering islanding operation constraints. IEEE Syst. J. **14**(4), 5340–5349 (2020). https://doi.org/10.1109/JSYST.2020.2964637
24. Chalil Madathil, S., Yamangil, E., Nagarajan, H., Barnes, A., Bent, R., Backhaus, S., Mason, S.J., Mashayekh, S., Stadler, M.: Resilient off-grid microgrids: capacity planning and n-1 security. IEEE Trans. Smart Grid **9**(6), 6511–6521 (2018). https://doi.org/10.1109/TSG.2017.2715074
25. Mashayekh, S., Stadler, M., Cardoso, G., Heleno, M., Madathil, S.C., Nagarajan, H., Bent, R., Mueller-Stoffels, M., Lu, X., Wang, J.: Security-constrained design of isolated multi-energy microgrids. IEEE Trans. Power Syst. **33**(3), 2452–2462 (2018). https://doi.org/10.1109/TPWRS.2017.2748060
26. Zhao, B., Zhang, X., Li, P., Wang, K., Xue, M., Wang, C.: Optimal sizing, operating strategy and operational experience of a stand-alone microgrid on Dongfushan Island. Appl. Energy **113**, 1656–1666 (2014). https://doi.org/10.1016/j.apenergy.2013.09.015
27. Yurdakul, O., Sivrikaya, F., Albayrak, S.: Quantification of the impact of GHG emissions on unit commitment in microgrids. In: 2020 IEEE PES Transmission and Distribution Conference and Exhibition—Latin America (TDLA), pp. 1–6 (2020). https://doi.org/10.1109/TDLA47668.2020.9326213
28. Bordin, C., Anuta, H.O., Crossland, A., Gutierrez, I.L., Dent, C.J., Vigo, D.: A linear programming approach for battery degradation analysis and optimization in offgrid power systems with solar energy integration. Renew. Energy **101**, 417–430 (2017). https://doi.org/10.1016/j.renene.2016.08.066
29. Marocco, P., Ferrero, D., Martelli, E., Santarelli, M., Lanzini, A.: An MILP approach for the optimal design of renewable battery-hydrogen energy systems for off-grid insular communities. Energy Convers. Manag. **245**, 114564 (2021). https://doi.org/10.1016/j.enconman.2021.114564
30. Salameh, T., Ghenai, C., Merabet, A., Alkasrawi, M.: Techno-economical optimization of an integrated stand-alone hybrid solar PV tracking and diesel generator power system in khorfakkan, united arab emirates. Energy **190**, 116475 (2020). https://doi.org/10.1016/j.energy.2019.116475
31. Shen, X., Han, Y., Zhu, S., Zheng, J., Li, Q., Nong, J.: Comprehensive power-supply planning for active distribution system considering cooling, heating and power load balance. J. Mod. Power Syst. Clean Energy **3**(4), 485–493 (2015). https://doi.org/10.1007/s40565-015-0164-5
32. Afzali, S.F., Mahalec, V.: Optimal design, operation and analytical criteria for determining optimal operating modes of a CCHP with fired HRSG, boiler, electric chiller and absorption chiller. Energy **139**, 1052–1065 (2017). https://doi.org/10.1016/j.energy.2017.08.029
33. Hampo, C.C., Akmar, A.B., Majid, M.A.A.: Life cycle assessment of an electric chiller integrated with a large district cooling plant. Sustainability **13**(1) (2021). https://doi.org/10.3390/su13010389
34. Fan, W., Liao, Y.: Microgrid operation optimization considering storage devices, electricity transactions and reserve. Int. J. Emerg. Electr. Power Syst. 20(5) (2019). https://doi.org/10.1515/ijeeps-2019-0003
35. Ghaljehei, M., Khorsand, M.: Day-ahead operational scheduling with enhanced flexible ramping product: design and analysis. IEEE Trans. Power Syst. **37**(3), 1842–1856 (2022). https://doi.org/10.1109/TPWRS.2021.3110712
36. He, L., Zhang, J., Hobbs, B.: Estimation of regulation reserve requirements in California ISO: a data-driven method. In: 2023 IEEE Power and Energy Society General Meeting (PESGM), pp. 1–5 (2023). https://doi.org/10.1109/PESGM52003.2023.10252917

37. Boyd, S., Vandenberghe, L.: Convex Optimization. Cambridge University Press, Cambridge (2004)
38. Ben-Tal, A., Ghaoui, L.E., Nemirovski, A.: Robust Optimization. Princeton Series in Applied Mathematics. Princeton University Press, Princeton (2009). https://books.google.com.co/books?id=DttjR7IpjUEC
39. Ben-Tal, A., Nemirovski, A.: Robust optimization? Methodology and applications. Math. Program. **92**(3), 453–480 (2002). https://doi.org/10.1007/s101070100286
40. Deforest, N., Cardoso, G., Brouhard, T., USDOE: distributed energy resources customer adoption model (DER-CAM) v5.9 (2018). https://doi.org/10.11578/dc.20181016.2. https://www.osti.gov/biblio/1477858
41. Jakhrani, A.Q., Rigit, A.R.H., Othman, A.-K., Samo, S.R., Kamboh, S.A.: Estimation of carbon footprints from diesel generator emissions. In: 2012 International Conference on Green and Ubiquitous Technology, pp. 78–81 (2012). https://doi.org/10.1109/GUT.2012.6344193
42. Chandrasekharam, D., Pathegama, G.R.: CO2 emissions from renewables: solar PV, hydrothermal and EGS sources. Geomech. Geophys. Geo-Energy Geo-Resour. **6**(1) (2019). https://doi.org/10.1007/s40948-019-00135-y
43. Hidrología, M.y.E.A.: Datos Hidrometeorológicos Crudos - Red de Estaciones IDEAM: Temperatura (2021). http://www.ideam.gov.co/
44. Engerer, N.: Global Solar Irradiance Data via API. The Australian National University Data Commons (2018). https://doi.org/10.25911/5c073e713e5dd. https://researchdata.edu.au/global-solar-irradiance-api. https://solcast.com.au/solar-data-api/api/terms-and-conditions/
45. Hart, W.E., Watson, J.-P., Woodruff, D.L.: PYOMO: modeling and solving mathematical programs in python. Math. Program. Comput. **3**(3), 219–260 (2011)
46. Gurobi Optimization, LLC: Gurobi Optimizer Reference Manual (2021)
47. Generator, S.: Approximate diesel generator fuel consumption chart. https://www.generatorsource.com/Diesel_Fuel_Consumption.aspx
48. Generator, S.: Approximate Natural Gas Consumption Chart. https://www.generatorsource.com/Natural_Gas_Fuel_Consumption.aspx
49. Units and calculators explained. https://www.eia.gov/energyexplained/units-and-calculators/

Authors and Affiliations

Juan Camilo Camargo-Berrueco[1] · Diego Adolfo Mejía-Giraldo[1] · Santiago Lemos-Cano[2]

✉ Juan Camilo Camargo-Berrueco
camilo.camargo@udea.edu.co

✉ Diego Adolfo Mejía-Giraldo
diego.mejia@udea.edu.co

Santiago Lemos-Cano
slemoscano@gmail.com

[1] Department of Electrical Engineering, Universidad de Antioquia, Calle 70 No. 52-21, Medellín 050010, Antioquia, Colombia

[2] Empresa de Energía del Pacífico S.A. E.S.P. (EPSA)-CELSIA S.A. E.S.P., Carrera 43A No. 1 sur-143, Medellín 050021, Antioquia, Colombia